Reprinted from ENGINEERING FOR POWER, *Vol. 98, No. 2, April 1976*

J. C. Nicholas
Research Associate.

E. J. Gunter
Associate Professor.

P. E. Allaire
Assistant Professor.

University of Virginia,
Charlottesville, Va.

Effect of Residual Shaft Bow on Unbalance Response and Balancing of a Single Mass Flexible Rotor

Part 1: Unbalance Response

The effect of residual shaft bow on the unbalance response of a single mass rotor on rigid supports has been examined with a theoretical analysis. The analysis determined the amplitude, phase angle, and peak rotor response speed for various combinations of residual bow and unbalance. For most combinations the phase angle corresponding to the peak rotor response speed was significantly different from the 90 degrees observed in the conventional unbowed rotor. If the residual bow and unbalance were exactly out of phase, the rotor amplitude was zero for a rotor speed equal to the square root of the ratio of residual bow amplitude to unbalance eccentricity. The results of the study suggested a simple method for determining the relative amplitudes of residual bow and unbalance eccentricity based upon the motion of a timing mark on an oscilliscope screen. If the residual bow was less than the unbalance eccentricity, the timing mark moved first in the direction of rotor rotation as the speed is increased and then moved in the opposite direction at a speed less than the critical speed. In the reverse situation, the timing mark moved opposite to the direction of rotation as the speed is increased. At some speed above the critical, it reversed direction. Part II of this paper presents theoretical and experimental results for balancing of a single mass rotor with a residual bow.

Introduction

The purpose of this paper is to analyze the effect of residual bow on the dynamic response of an unbalanced single mass (Jeffcott) rotor on rigid supports. The results of this analysis are used to suggest improvements in balancing technique for high speed rotating machinery.

In many rotor applications there can exist a residual bow in the shaft due to various effects such as thermal distortion, gravity sag, mechanical bow resulting from prior unbalance, or shrink fits. Some of these are temporary while others are permanent in nature.

During the start up of hot turbomachinery, such as gas turbines, steam turbines and water pumps in nuclear reactors, a bow can be developed in the rotor shaft due to an asymmetric heat distribution. This may be caused by partial steam inlet conditions in a steam turbine. The rotor must be slowly brought up to speed while being uniformly heated to avoid inducing a large thermal bow. This may require several days for some of the very large steam turbines.

Another problem arises in large horizontal turbines or compressors which are allowed to sit for long periods of time. The gravitational sag of the rotor may produce a temporary mechanical bow in the shaft. Upon start up the bowed shaft may cause large vibrational amplitudes due to the combination of residual bow and rotor unbalance.

Longer lasting sources of residual bow arise from shrink fits and thermal bows due to the rubbing of a shaft on a seal. The shrink fit of the rotor to the shaft may produce a permanent mechanical bow in the shaft. Thermal bow due to shaft rubbing was reported by Newkirk [1][1] and recently investigated by Dimarogonas [2]. If this effect occurs below critical speed, the residual bow tends to increase which in turn increases the rubbing effect. The motion is unstable and can lead to catastrophic failure of the rotor system if the vibration is unchecked.

Dimarogonas [2], Kikuchi [3], and Yamamoto [4] have all discussed the problem of a warped shaft due to thermal effects. As yet however, there has been little reported information on the rotor

Contributed by the Gas Turbine Division and presented at the Gas Turbine Conference, Houston, Texas, March 2–6, 1975, of THE AMERICAN SOCIETY OF MECHANICAL ENGINEERS. Manuscript received at ASME Headquarters, December 2, 1974. Paper No. 75-GT-48.

[1] Numbers in brackets designate References at end of paper.

amplitude and phase angle change due to residual bow. In the practical application of balancing of turbo machinery, it is very important to understand the influence of residual shaft deflection in order to properly balance the rotor system. Improper placement of the balancing weight can make the unbalance worse than original case.

It has been found that the rotor phase angle with a bowed shaft will be considerably different than the predicted phase angle with the normal single mass model. Discussion with several persons in industry on phase angle measurements has indicated that because of the peculiar phase angle data observed, they were hesitant to print this material because they were unable to explain the phenomena. Therefore one objective of this paper is to not only explain the dynamic unbalance response but also the type of phase angle changes that may be expected with a bowed shaft.

The results and conclusions obtained for the dynamic unbalance response and balancing of the single mass rotor may be applied to multistage centrifugal compressors and turbines by means of modal analysis. From the calculation of the rotor first critical speed and mode shape, an equivalent modal mass and effective shaft stiffness may be calculated.

Some turbo machinery, e.g., high-pressure multistage compressors of barrel construction, have easy access only at the rotor ends. Therefore, in the field, they can be balanced only in two planes. According to Sternlicht [5], these machines should be designed to operate below the second critical speed. Thus a single mass model is directly applicable to this type of machine.

Part I of this paper deals with a theoretical analysis of a single mass rotor with a bowed shaft. Part II presents theoretical and experimental results on balancing of such a rotor.

1 Dynamic Response of Bowed Rotor

1.1 Equations of Motion. A single disk is mounted at the center of a uniform flexible shaft as shown in Fig. 1. The shaft has a residual bow of magnitude δ_r and phase angle ϕ_r. The mass center of the disk is displaced a distance e_u from the shaft center line which results in a dynamic bow as the shaft rotates. Its magnitude and phase angle are δ_s and ϕ_s, respectively. Thus the total shaft bow is

$$\vec{\delta} = \vec{\delta}_r + \vec{\delta}_s \tag{1}$$

No gyroscopic effects occur since the disk always rotates in its own plane. The shaft mass is small compared to the disk mass. Both the shaft and disk rotate with constant angular velocity ω. The supports are taken as rigid (no spring or dampers act at the bearings).

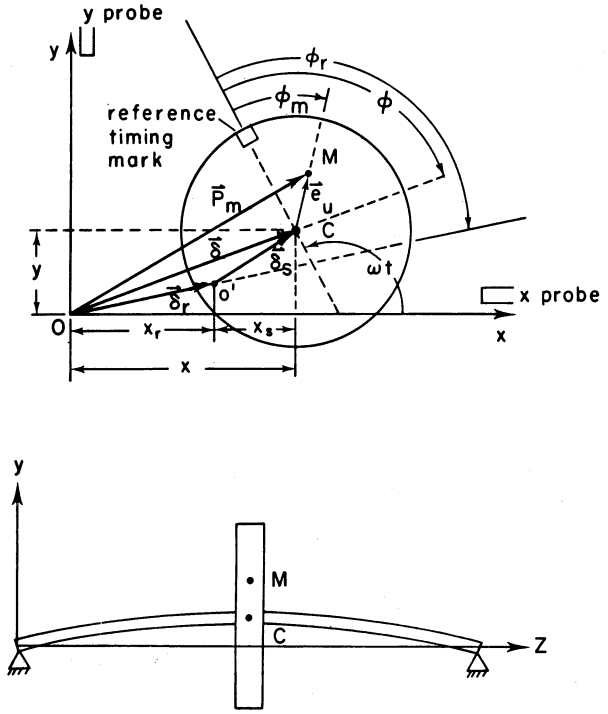

Fig. 1 Single mass flexible rotor with bowed shaft, end and side views

D'Alembert's principle is used to formulate the equations of motion for the rotating disk with the residual shaft bow. The position vector $\mathbf{P}_m$ from the unbowed, nonrotating center line of the shaft to the mass center, M, of the disk is

$$\mathbf{P}_m = \vec{\delta} + \mathbf{e}_u \tag{2}$$

If the cartesian coordinates of the center line are denoted by x and y, equation (2) gives

$$\mathbf{P}_m = [x + e_u \cos(\omega t - \phi_m)]\mathbf{i} + [y + e_u \sin(\omega t - \phi_m)]\mathbf{j} \tag{3}$$

The acceleration of the mass center is

$$\mathbf{a}_m = [\ddot{x} - \omega^2 e_u \cos(\omega t - \phi_m)]\mathbf{i} + [\ddot{y} - \omega^2 e_u \sin(\omega t - \phi_m)]\mathbf{j} \tag{4}$$

where the dots denote differentiation with respect to time.

By D'Alembert's principle, the sum of external forces plus exter-

Nomenclature

A = amplification factor, $|\bar{Z}| = \delta/e_u$, dim
A_{cr} = amplification factor at rotor critical speed, dim
$A_{\max}$ = maximum amplification factor, dim
$\mathbf{a}_m$ = acceleration of rotor mass center
c = shaft damping, N-s/cm (lb-s/in.)
c_{cr} = critical damping coefficient, N-s/cm (lb-s/in.)
$\mathbf{e}_u$ = unbalance eccentricity vector
e_u = unbalance eccentricity, $|\mathbf{e}_u|$, cm (in.)
f = frequency ratio, ω/ω_{cr}, dim
$f_{\max}$ = frequency ratio at maximum amplitude, dim
k = shaft spring rate, N/cm (lb/in.)
m = rotor mass, N-s^2/cm (lb-s^2/in.)
N = rotor speed, rpm
$\mathbf{P}_m$ = position vector of rotor mass center
t = time, s
x = horizontal shaft center line displacement
y = vertical shaft center line displacement
z = complex shaft center line displacement, $x + iy$
Z = complex amplitude of motion (steady-state response)
$\bar{Z}$ = nondimensional, complex amplitude, Z/e_u
$\bar{Z}_{cr}$ = nondimensional, complex amplitude at rotor critical speed
$\bar{Z}_r$ = real part of $\bar{Z}$
$\bar{Z}_i$ = imaginary part of $\bar{Z}$
γ = angle between the residual bow vector $\vec{\delta}_r$ and the mass unbalance vector $\mathbf{e}_u$
$\vec{\delta}$ = shaft center line deflection vector
δ = shaft center line deflection, $|\vec{\delta}|$, cm (in.)
$\vec{\delta}_r$ = residual bow vector
δ_r = residual bow, $|\vec{\delta}_r|$, cm (in.)
$\bar{\delta}_r$ = nondimensional residual bow, δ_r/e_u
$\vec{\delta}_s$ = elastic shaft deflection vector
ξ = damping ratio, c/c_{cr}, dim
ϕ = phase angle between the shaft center line vector $\vec{\delta}$ and the shaft reference timing mark
ϕ_{cr} = phase angle ϕ at rotor critical speed
$\phi_{\max}$ = phase angle ϕ at maximum amplitude
ϕ_m = angle between mass center and shaft reference timing mark
ϕ_r = angle between residual bow vector $\vec{\delta}_r$ and the shaft reference timing mark
ω = shaft angular velocity, rad/s
ω_{cr} = rotor critical speed, $\sqrt{k/m}$, rad/s

nally applied forces must vanish. The inertia force acting on the disk is

$$-m\mathbf{a}_m$$

An externally applied (so far as the disk is concerned) elastic restoring force

$$-k\vec{\delta}_s$$

acts to return the shaft center line to the residual bowed position due to the shaft stiffness. Also a damping force

$$-c\dot{\vec{\delta}}$$

acts at the disk to return the shaft center line to the unbowed, nonrotating position. The equation of motion is

$$m\mathbf{a}_m + c\dot{\vec{\delta}} + k\vec{\delta}_s = 0 \tag{5}$$

or in terms of x and y from equations (1) and (4)

$$m\{\ddot{x} - \omega^2 e_u \cos(\omega t - \phi_m)\} + c\dot{x} + k\{x - \delta_r \cos(\omega t - \phi_r)\} = 0 \tag{6}$$

$$m\{\ddot{y} - \omega^2 e_u \sin(\omega t - \phi_m)\} + c\dot{y} + k\{y - \delta_r \sin(\omega t - \phi_r)\} = 0 \tag{7}$$

These two second order differential equations describe the dynamic response of the shaft center line.

For convenience, the shaft center line position z in complex form is defined as

$$z = x + iy$$

The result of multiplying equation (7) by i and adding it to equation (6) is

$$m\{\ddot{z} - \omega^2 e_u e^{i(\omega t - \phi_m)}\} + c\dot{z} + k\{z - \delta_r e^{i(\omega t - \phi_r)}\} = 0$$

1.2 Steady State Unbalance Response. Solving for z

$$m\ddot{z} + c\dot{z} + kz = m\omega^2 e_u e^{i(\omega t - \phi_m)} + k\delta_r e^{i(\omega t - \phi_r)} \tag{8}$$

For constant angular velocity, assume a solution of the form

$$z = Ze^{i\omega t}$$

where Z is the complex amplitude of motion. The result is

$$Z = \frac{m\omega^2 e_u e^{-i\phi_m} + k\delta_r e^{-i\phi_r}}{-m\omega^2 + ic\omega + k} \tag{9}$$

This describes the rotor amplitude of motion of steady-state circular synchronous precession.

The dynamic response of the residually bowed rotor can be more easily examined with the introduction of dimensionless parameters. Let the critical speed, ω_{cr}, of the undamped rotor ($c \to 0$) be given by the well known relation

$$\omega_{cr}^2 = \frac{k}{m}$$

and the critical damping, c_{cr}, be given by

$$c_{cr} = 2m\omega_{cr}$$

The dimensionless frequency ratio, f, and damping ratio, ξ, can be defined as

$$f = \frac{\omega}{\omega_{cr}}$$

$$\xi = \frac{c}{c_{cr}}$$

For these variables, the complex dimensionless rotor amplitude is

$$\overline{Z} = \frac{\overline{\delta}_r e^{-i\phi_r} + f^2 e^{-i\phi_m}}{1 - f^2 + 2i\xi f} \tag{10}$$

where

$$\overline{Z} = \frac{Z}{e_u}$$

$$\overline{\delta}_r = \frac{\delta_r}{e_u}$$

The complex amplification factor, $\overline{Z}$, gives the amplitude and phase angle of the dynamic response of the shaft center line due to residual shaft bow and mass unbalance for steady state circular synchronous precession.

The full solution for z is

$$\frac{z}{e_u} = \frac{\overline{\delta}_r e^{i(\omega t - \phi_r)} + f^2 e^{i(\omega t - \phi_m)}}{1 - f^2 + 2i\xi f} \tag{11}$$

Equation (10) is of greater interest.

1.3 Rotor Amplification Factor and Phase Angles. For convenience, let γ be the angle by which the residual bow vector $\vec{\delta}_r$ leads the mass unbalance vector $\mathbf{e}_u$

$$\gamma = \phi_r - \phi_m$$

Then equation (10) becomes

$$\overline{Z} = \frac{\overline{\delta}_r e^{-i\gamma} + f^2}{1 - f^2 + 2i\xi f} e^{-i\phi_m} \tag{12}$$

Without loss of generality the shaft reference mark can be taken in phase with the mass unbalance vector or $\phi_m = 0$ and $\phi_r = \gamma$.

$$\overline{Z} = \frac{\overline{\delta}_r e^{-i\gamma} + f^2}{1 - f^2 + 2i\xi f} \tag{13}$$

This expression shows that the two most important variables for the residual bow are the ratio of residual bow amplitude to mass unbalance, $\bar{\delta}_r$, and the phase angle γ.

The complex rotor amplification factor is related to the shaft amplitude of motion, δ, and phase angle, ϕ, by

$$\overline{Z} = Ae^{-i\phi}$$

where A is the amplification factor ($A = \delta/e_u$). Separating $\overline{Z}$ into real and imaginary components

$$\overline{Z} = \overline{Z}_r + i\overline{Z}_i$$

Equation (13) gives

$$\overline{Z}_r = \frac{(\overline{\delta}_r \cos\gamma + f^2)(1 - f^2) - 2\xi f\overline{\delta}_r \sin\gamma}{(1 - f^2)^2 + (2\xi f)^2} \tag{14}$$

$$\overline{Z}_i = \frac{\overline{\delta}_r \sin\gamma(1 - f^2) + 2\xi f(\overline{\delta}_r \cos\gamma + f^2)}{(1 - f^2)^2 + (2\xi f)^2} \tag{15}$$

The shaft amplification factor and phase angle are given by

$$A = |\overline{Z}| = \sqrt{\overline{Z}_r^2 + \overline{Z}_i^2} \tag{16}$$

$$\phi = \tan^{-1}\left(-\frac{\overline{Z}_i}{\overline{Z}_r}\right) \tag{17}$$

Curves showing the variation of A and ϕ with speed for various values of residual bow, phase angle, and damping are given in Section 2.

1.4 Critical Speed and Maximum Rotor Amplification Factor. At the critical speed, the complex amplification factor is

$$\overline{Z}_{cr} = \frac{\overline{\delta}_r e^{-i\gamma} + 1}{2\xi i} \tag{18}$$

Equations (14) and (15) reduce to

$$\overline{Z}_r = -\frac{\overline{\delta}_r \sin\gamma}{2\xi}$$

$$\overline{Z}_i = -\frac{\overline{\delta}_r \cos\gamma + 1}{2\xi}$$

and the amplification factor, A_{cr}, and phase angle, ϕ_{cr}, are

$$A_{cr} = \frac{1}{2\xi}\sqrt{(\bar{\delta}_r \cos\gamma + 1)^2 + (\bar{\delta}_r \sin\gamma)^2} \quad (19)$$

$$\phi_{cr} = \tan^{-1}\left(-\frac{\bar{\delta}_r \cos\gamma + 1}{\bar{\delta}_r \sin\gamma}\right) \quad (20)$$

For an unbowed rotor the critical amplification factor reduces to the familiar value

$$A_{cr} = \frac{1}{2\xi}, \bar{\delta}_r \longrightarrow 0$$

The phase angle for the unbowed rotor is 90 deg as the denominator of equation (20) vanishes.

If the rotor has some residual bow, $\bar{\delta}_r$ does not vanish. The critical speed phase angle is 90 deg only when the residual bow vector is in phase with the mass unbalance vector (γ = 0 deg) or exactly out of phase (γ = 180 deg). For example, when the bow phase angle is 90 deg

$$A_{cr} = \frac{1}{2\xi}\sqrt{1 + \bar{\delta}_r^2} \quad (21)$$

$$\phi_{cr} = \tan^{-1}\left(-\frac{1}{\bar{\delta}_r}\right) \quad (22)$$

Even a relatively small residual bow, $\bar{\delta}_r$ = 0.5, produces a 116.5 deg phase angle at the critical speed rather than the normal 90 deg phase for an unbowed rotor.

It is also of interest to compute the frequency ratio, f_{max}, at which the amplification factor has a maximum or minimum. Evaluating

$$\frac{dA}{dF} = 0$$

from equations (14), (15), and (16) and solving for f gives

$$f_{max}^2 = \frac{\bar{\delta}_r^2 - 1 \pm \sqrt{(\bar{\delta}_r^2 - 1)^2 - 4(-1 + 2\xi^2 - \bar{\delta}_r \cos\gamma)(\bar{\delta}_r \cos\gamma + \bar{\delta}_r^2 - 2\xi^2\bar{\delta}_r^2)}}{2(-1 + 2\xi^2 - \bar{\delta}_r \cos\gamma)} \quad (23)$$

The maximum (or minimum) amplification factor may occur at two different frequencies. For example consider $\bar{\delta}_r$ = 0.5, the two frequencies given by equation (23) are 0.0 and 1.414. This is the critically damped case where f_{max} = 1.414 is a minimum. If the damping ratio is ξ = 0.3, the two frequencies are 0.740 and 1.414 which are a maximum and minimum, respectively. These results are shown in detail in Section 2.

Equation (16) may also be written as

$$A = \frac{\sqrt{(\bar{\delta}_r \cos\gamma + f^2)^2 + (\bar{\delta}_r \sin\gamma)^2}}{\sqrt{(1 - f^2)^2 + (2\xi f)^2}} \quad (24)$$

Note that if γ is 180 deg this expression reduces to

$$A = \frac{f^2 - \bar{\delta}_r}{\sqrt{(1 - f^2)^2 + (2\xi f)^2}} \quad (25)$$

Clearly, the amplitude is zero when $f = \sqrt{\bar{\delta}_r}$ independent of the damping ratio.

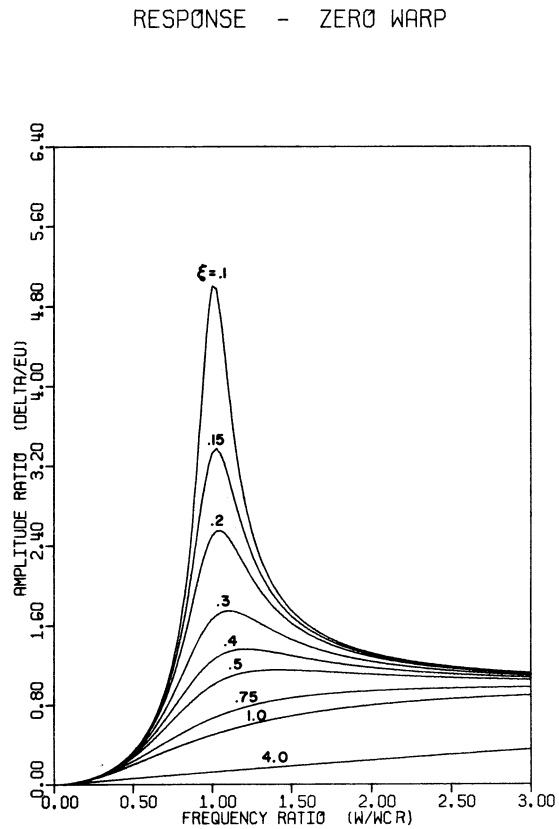

Fig. 2 Response curves with zero residual warp for various damping ratios

2 Dynamic Unbalance Response for the Bowed Shaft-Amplitude and Phase Angle

2.1 Rotor Response With No Residual Bow. The dynamic unbalance response and phase angles for the single mass Jeffcott rotor on rigid supports with a bowed shaft is given by equations (16) and (17). In *all* response curves that follow, the amplitude ratio is made dimensionless with respect to the shaft unbalance eccentricity e_u. The first set of curves generated are shown in Figs. 2 and 3 which correspond to the rotor amplitudes and phase angles of the single mass rotor with no residual shaft bow for values of damping ratio varying from 0.1 to 4.0. The value of 0.5 represents critical damping in which the critical speed is not excited. From the observation of the amplitude versus speed curves, it can be seen that as the damping is increased the response changes significantly. For damping ratios above 0.5, the maximum amplitude of the single mass rotor without shaft bow occurs at frequency ratio above 1.0. It is of interest to observe that when the shaft bow is introduced this will not be the case.

Fig. 3 represents the rotor phase angle versus speed ratio for various values of damping. The results shown in Figs. 2 and 3 on rotor amplitude and phase angle are well known and have been previously reported. The original equations describing the rotor unbalance and phase angle change were first presented by H. H. Jeffcott [6] in 1919 and the curves for rotor amplitude and phase angle have been shown by Thomson [7], Myklestad [8], and others [9, 10].

For very low values of damping the rotor phase angle below the critical speed will be approximately 0 deg. This means that the rotor mass center is in line with the deflection of the rotor. From Fig. 3 it is obvious that regardless of the damping value, the phase angle will be 90 deg at the critical speed (f = 1). For a lightly damped rotor the phase angle will change to almost 180 deg when the critical speed is exceeded. Numerous people have used the 90 deg phase angle shift as an indication that they are observing a critical speed response. It is important to note that the phase angle change at the critical speed with a bowed shaft will not necessarily correspond to 90 deg.

Table 1 represents the critical and maximum values of amplification factors and phase angles for various damping ratios. Note that for the case of low damping (ξ = 0.10) where the rotor critical amplification factor A_{cr} = 5, the maximum amplitude A_{max} is only 0.5 percent larger than the critical amplification factor. Furthermore, it occurs at a speed of only 1 percent higher than the undamped critical speed. However, the corresponding phase angle at

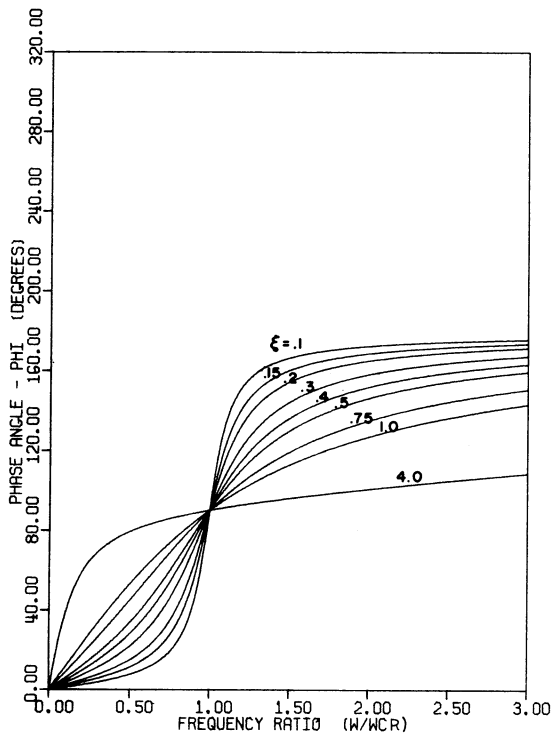

Fig. 3 Phase angle curves with zero residual warp for various damping ratios

maximum amplitude is not 90 deg but 96 deg, a 6 deg phase shift from ϕ_{cr}. This can have an important effect on balancing in field use when the amplitude and phase angle method of balancing at the critical speed is used. The mass center, therefore is not leading the amplitude vector by 90 deg as is commonly assumed but is leading by the values given in Table 1. As damping on the rotor increases, this phase angle discrepancy between ϕ_{cr} and $\phi_{\max}$ also increases up to $\phi_{\max} = 125$ deg for critical damping ($\xi = 0.5$).

For a heavily damped rotor, with an amplification factor of approximately 2, the frequency at which the maximum amplitude occurs may be as great as 10 percent above $f = 1.0$. Above critical damping ($\xi > 0.5$) the rotor amplitude continues to increase with speed and the values of $A_{\max}$ and $\phi_{\max}$ will approach asmptotically the values of 1 and 180 deg respectively as $f \rightarrow \infty$.

2.2 Rotor Response With Small Residual Bow $-\bar{\delta}_r = 0.5$. In the set of amplitude and phase angle curves represented by Figs. 4–7, the shaft bow was assumed to be equal to one half of the rotor unbalance eccentricity ($\bar{\delta}_r = 0.5$). Fig. 4 represents rotor response curves for $\phi_r = 90$ deg (unbalance eccentricity vector leading the residual bow vector by 90 deg). At low speeds, considerably below the rotor critical speed, the elastic deflection of the shaft may be considered negligible. If noncontacting proximity probes were placed adjacent to the shaft in the vicinity of the disk, then the shaft amplitude at low speed would correspond to the residual bow of the shaft. In Fig. 4 this would represent the dimensionless amplitude of 0.5 as shown for speeds less than 10 percent of the critical speed. The amplitude at zero frequency for the straight shaft as recorded by the noncontracting probes would be 0. Critical damping occurs at $\xi = 0.75$. The effect of excessive damping can easily be seen from the damping ratio $\xi = 4.0$ curve. The rotor amplitude diminishes and reaches a minimum at the frequency of approximately 0.7. After that the amplitude increases until it reaches the asymptotic value of 1. The amplitude value of 1 as $f \rightarrow \infty$ implies that the mass center lies along the axis of rotation of the rotor. The maximum amplitude ratio is 5.6 (for $\xi = 0.1$). For the

Table 1 Critical and maximum values of amplification factors and phase angles for various damping ratios—zero shaft warp ($\bar{\delta}_r = 0$)

$\bar{\delta}_r = 0$

ξ	A_{cr}	A_{max}	ϕ_{cr}	ϕ_{max}	f_{max}
.10	5.000	5.025	90.00	95.77	1.0102
.15	3.333	3.371	90.00	98.73	1.0233
.20	2.500	2.552	90.00	101.78	1.0426
.30	1.667	1.747	90.00	108.33	1.1043
.40	1.250	1.364	90.00	115.88	1.2127
.50	1.000	1.155	90.00	125.26	1.4142
.75	.667	1.000	90.00	180.00	∞
1.00	.500	1.000	90.00	180.00	∞
4.00	.125	1.000	90.00	180.00	∞

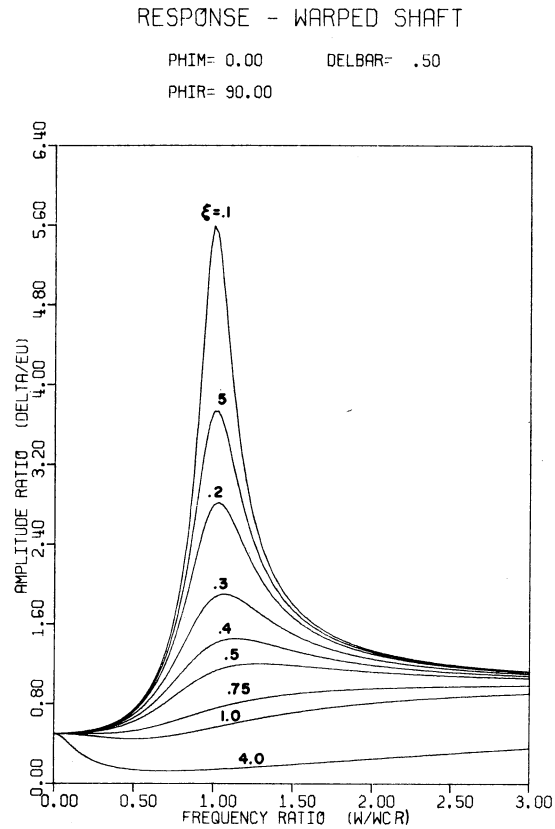

Fig. 4 Response curves with $\bar{\delta}_r = 0.5$, $\phi_r = 90$ deg for various damping ratios

zero warp case, the maximum amplitude ratio was approximately 5.0 (again for $\xi = 0.1$). In fact, the response curves for $\bar{\delta}_r = 0.5$ and $\phi_r = 90$ deg are very similar to the classical response curves for the zero warp case. The only major difference is that all curves start at a value of 0.5 for the $\bar{\delta}_r = 0.5$ and $\phi_r = 90$ deg case whereas the response curves for zero warp start at zero.

Fig. 5 shows the phase angle curves for the $\bar{\delta}_r = 0.5$, $\phi_r = 90$ deg case. It is clear that while the corresponding response curves are very similar to the zero warp case, the phase angle curves are very different especially in the region between $f = 0$ and $f = 1$. The phase angle is 90 deg for $f = 0$ as expected since $\phi_r = 90$ deg. However, for damping ratios between $\xi = 0.1$ and $\xi = 0.5$, the phase angle decreases before it increases to a value of $\phi_{cr} = 116.56$ deg at $f = 1$. For the over damped cases ($\xi = 1.0, 4.0$), the phase angle in-

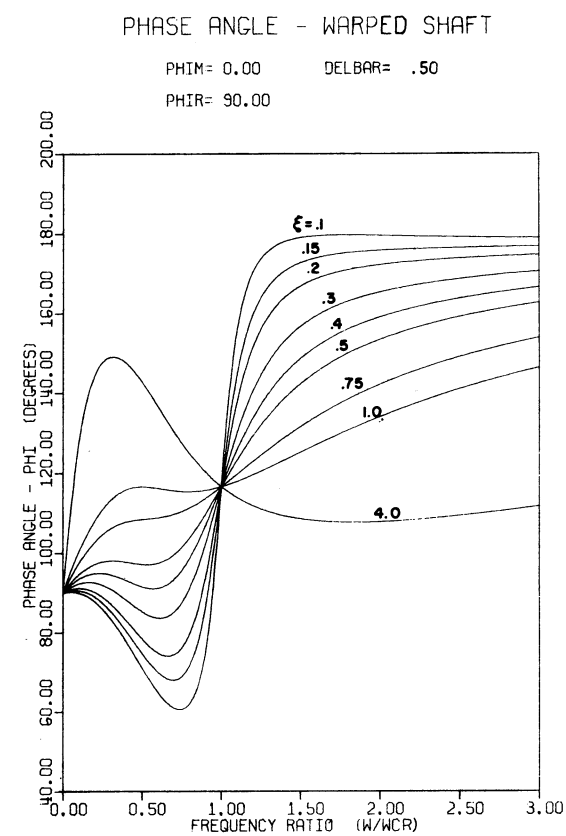

Fig. 5 Phase angle curves with $\bar{\delta}_r = 0.5$, $\phi_r = 90$ deg for various damping ratios

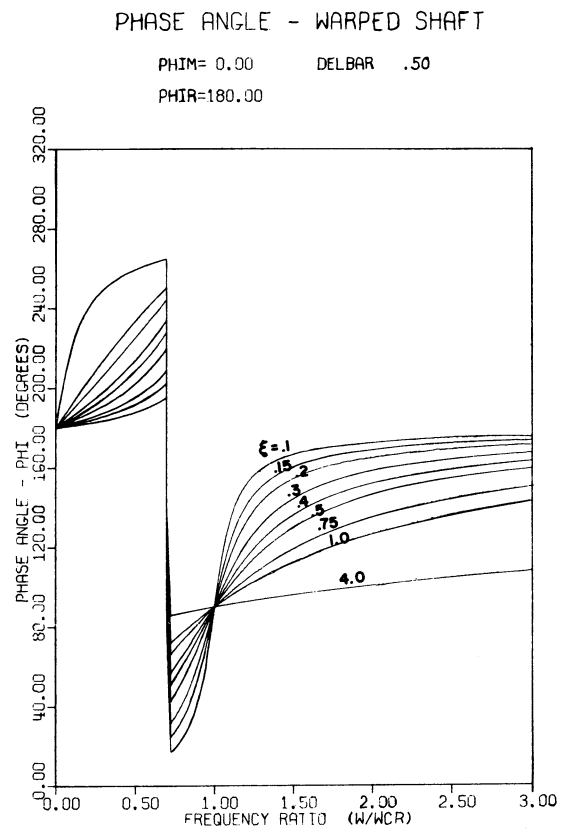

Fig. 7 Phase angle curves with $\bar{\delta}_r = 0.5$, $\phi_r = 180$ deg for various damping ratios

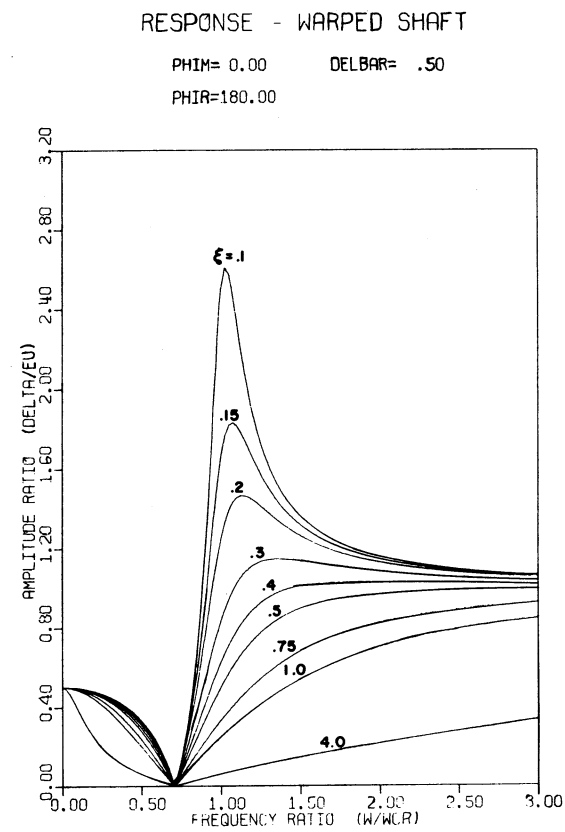

Fig. 6 Response curves with $\bar{\delta}_r = 0.5$, $\phi_r = 180$ deg for various damping ratios

creases before it decreases to ϕ_{cr}. This does not occur for zero warp where the phase angle increases steadily from $\phi = 0$ to $\phi_{cr} = 90$ deg. This is normally the way the phase angle is thought to behave. As seen here, this is not always the case. Also, note that $\phi_{cr} = 116.56$ deg for all damping values. As $f \rightarrow \infty$, all phase angle curves approach 180 deg as in the zero warp case.

Figs. 6 and 7 represent the rotor response and phase angle curves for $\bar{\delta}_r = 0.5$ and $\phi_r = 180$ deg (unbalance eccentricity vector leading the residual bow by 180 deg). From the response curve (Fig. 6), the maximum amplitude is 2.6 (for $\xi = 0.1$), considerably lower than any case seen thus far. This is intuitively obvious since the unbalance counteracts the residual warp thus reducing the amplitude ratio for all damping ratios. The rotor is balanced at a frequency ratio equal to the square root of $\bar{\delta}_r$ ($f = 0.7071$).

From Fig. 7, an abrupt 180 deg phase shift occurs at $f = 0.7071$ for all damping ratios. Fig. 8 shows the vector diagrams portraying this 180 deg shift. For very slow speeds, the shaft center line displacement vector $\vec{\delta}$ leads the unbalance vector $\mathbf{e}_u$ by 180 deg (see Fig. 8–1). As the speed increases, the unbalance tends to straighten the residual warp thus decreasing the magnitude of the displacement vector $\vec{\delta}$. At the same time, the phase angle increases slightly (Fig. 8–2). At a frequency ratio slightly less than $f = 0.7071$, the magnitude of $\vec{\delta}$ is very small while ϕ is approximately 195 deg (Fig. 8–3). When $f = 0.7071$, the unbalance has completely straightened the shaft. Now $\vec{\delta} = 0$ and the phase angle is undefined. At a frequency ratio slightly above $f = 0.7071$, the magnitude of $\vec{\delta}$ is very small but the direction has changed by 180 deg. Now the phase angle is approximately 15 deg (Fig. 8–4). For frequency ratios above $f = 0.7071$, the phase angle curves behave similarly to the standard phase plots for zero warp.

Fig. 9 shows how the response curves change for one specific value of damping ($\xi = 0.3$) as ϕ_r changes. All curves are for $\bar{\delta}_r = 0.5$. As ϕ_r increases from 90 deg to 180 deg, the maximum amplitude ratio decreases from about 1.9 to about 1.2. At $f = 0.7071$ (square

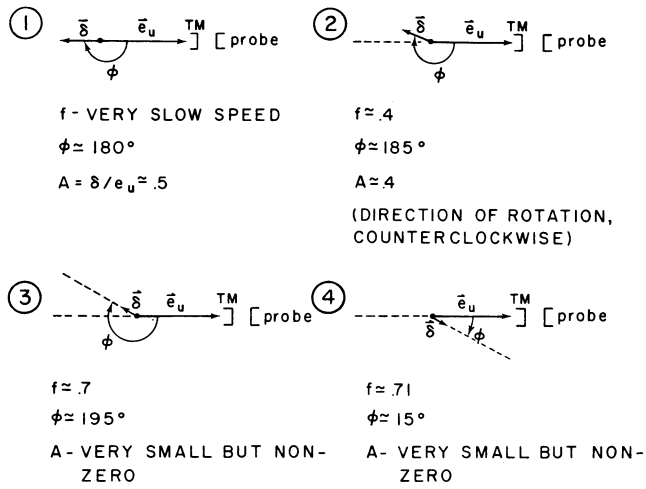

Fig. 8 Vector diagrams showing the 180 deg phase shift at $f = 0.7071$ for $\bar{\delta}_r = 0.5$, $\phi_r = 180$ deg

root of $\bar{\delta}_r$), the amplitude decreases to zero as $\phi_r \rightarrow 180$ deg.

Fig. 10 shows the corresponding phase angle plots ($\bar{\delta}_r = 0.5$, $\xi = 0.3$). It is clear that the abrupt 180 deg phase shift for $\phi_r = 180$ deg is the limiting case. For $\phi_r = 175$ deg, the phase angle curve is continuous across $f = 0.7071$ but very close to approaching a 180 deg phase shift at $f = 0.7071$.

Table 2 represents the critical and maximum values of amplification factors and phase angles for $\bar{\delta}_r = 0.5$ and $\phi_r = 180$ deg. For $\xi = 0.1$, $\phi_{cr} = 90$ deg and $\phi_{max} = 106.87$ deg (an increase of 16.87 deg). For zero shaft warp the phase angle shift was 6 deg. Thus, a

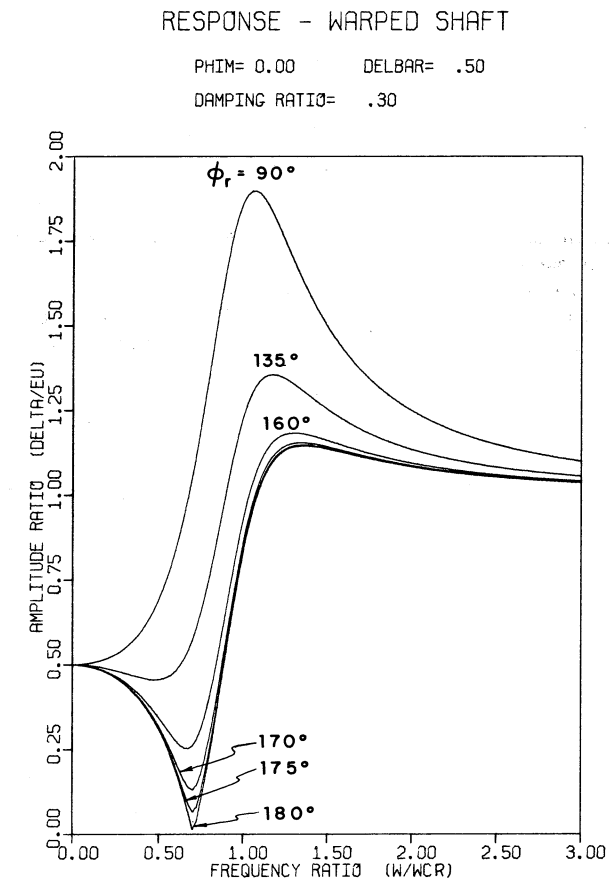

Fig. 9 Response curves with $\bar{\delta}_r = 0.5$, $\xi = 0.3$ for various ϕ_r values

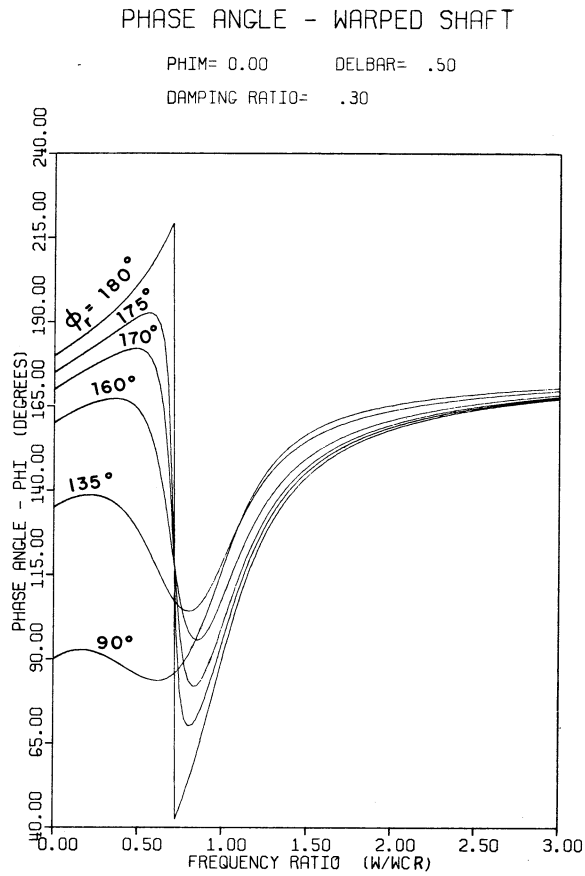

Fig. 10 Phase angle curves with $\bar{\delta}_r = 0.5$, $\xi = 0.3$ for various ϕ_r values

shaft warp equal to ½ the unbalance eccentricity and 180 deg out of phase with the unbalance eccentricity tends to increase the phase angle shift from ϕ_{cr} to ϕ_{max}. For $\xi = 0.4$, the phase angle shifts about 60 deg from 90 deg to 150 deg.

2.3 Rotor Response With Large Residual Bow $-\bar{\delta}_r = 2.0$. In the set of amplitude and phase angle curves represented by Figs. 11–13, the shaft bow is twice the rotor unbalance eccentricity ($\bar{\delta}_r = 2.0$). Since $\bar{\delta}_r$ has been increased, a corresponding increase in amplitude ratio should be expected. This may be seen to be true from Fig. 11 which represents the response curves for $\bar{\delta}_r = 2.0$ and $\phi_r = 180$ deg. The maximum amplitude ratio is 5.22 compared to 2.61 for the $\bar{\delta}_r = 0.5$, $\phi_r = 180$ deg case. The rotor is balanced at a frequency ratio of 1.414 (square root of $\bar{\delta}_r = 2.0$).

Table 2 Critical and maximum values of amplification factors and phase angles for various damping ratios ($\bar{\delta}_r = 0.5$, $\phi_r = 180$ deg)

$\bar{\delta}_r = .5$ $\quad \phi_r = 180.0°$

ξ	A_{cr}	A_{max}	ϕ_{cr}	ϕ_{max}	f_{max}
.10	2.500	2.611	90.00	106.87	1.0308
.15	1.667	1.831	90.00	114.77	1.0716
.20	1.250	1.466	90.00	122.21	1.1339
.30	.833	1.146	90.00	136.00	1.3578
.40	.625	1.030	90.00	150.12	1.9148
.50	.500	1.000	90.00	180.00	∞
.75	.333	1.000	90.00	180.00	∞
1.00	.250	1.000	90.00	180.00	∞
4.00	.063	1.000	90.00	180.00	∞

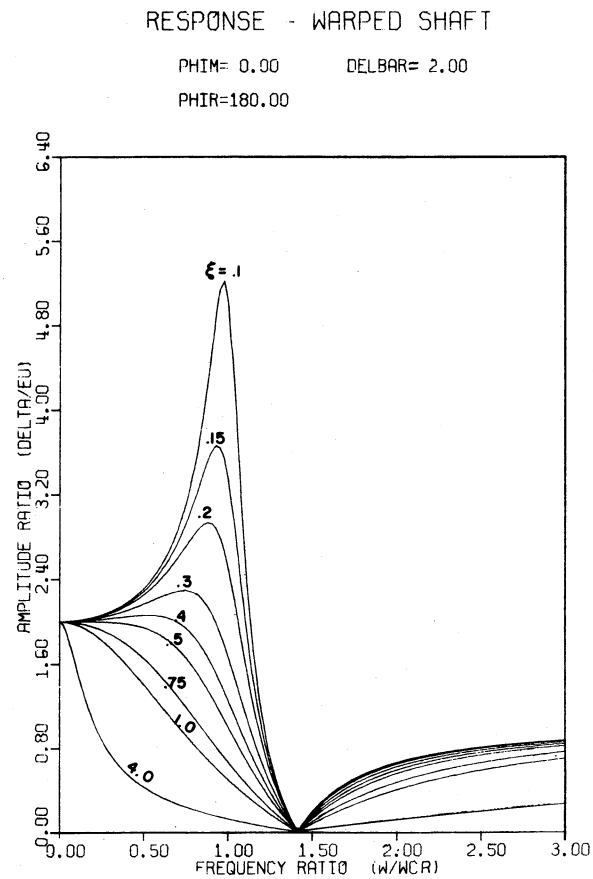

Fig. 11 Response curves with $\bar{\delta}_r = 2.0$, $\phi_r = 180$ deg for various damping ratios

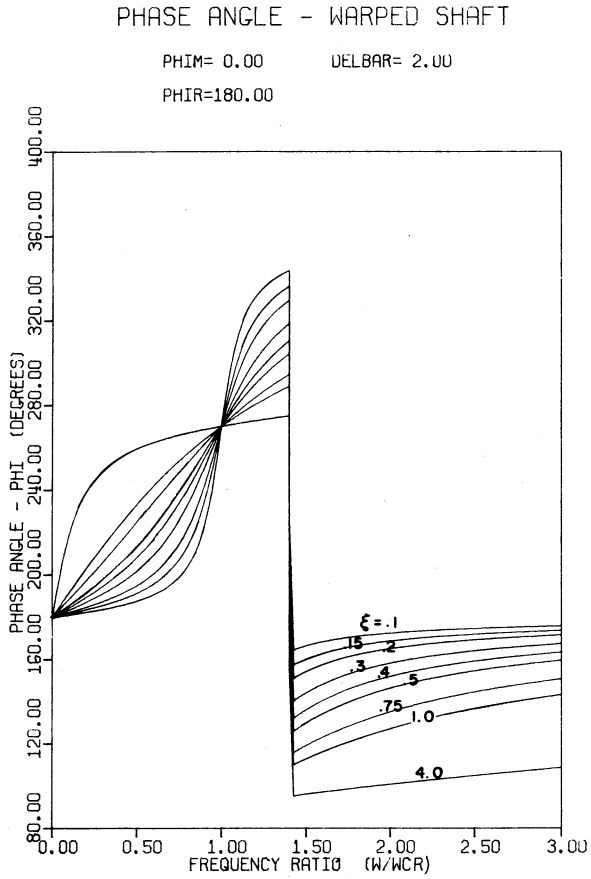

Fig. 12 Phase angle curves with $\bar{\delta}_r = 2.0$, $\phi_r = 180$ deg for various damping ratios

Fig. 12 which represents the phase angle curves for $\bar{\delta}_r = 2.0$ and $\phi_r = 180$ deg, indicates an abrupt 180 deg phase shift at $f = 1.414$. This shift occurs for the same reason that the 180 deg shift occured for $\phi_r = 180$ deg and $\bar{\delta}_r = 0.5$. Note that for frequency ratios between $f = 0$ and $f = 1.414$, the phase angle curves look very similar to the conventional phase plots for zero warp (see Fig. 3) except that they are all displaced by 180 deg. For frequency ratios above $f = 1.414$, the phase plots also behave conventionally since they approach 180 deg as $f \rightarrow \infty$.

From Table 3, which compares the critical and maximum amplification factors and phase angles for $\bar{\delta}_r = 2.0$ and $\phi_r = 180$ deg, $\phi_{cr} = 270$ deg. For a damping ratio of 0.1, $\phi_{cr} = 270$ deg while the phase angle at maximum amplification decreased to $\phi_{\max} = 253.13$ deg (a 16.87 deg decrease). Comparison of Table 2 for $\bar{\delta}_r = 0.5$ shows that the magnitude of the phase shifts are the same for all damping ratios. When $\bar{\delta}_r = 2.0$, the phase at maximum amplitude decreased from ϕ_{cr} while for $\bar{\delta}_r = 0.5$, $\phi_{\max}$ increased from ϕ_{cr}.

Fig. 13 represents phase angle plots for $\bar{\delta}_r = 2.0$ and $\phi_r = 135$ deg. Note that, for frequency ratios above $f = 1.0$, the phase angle curves for small damping ratios increase to values above 180 deg before they approach 180 deg as $f \rightarrow \infty$. In fact, at $f = 1.0$, $\phi_{cr} = 195$ deg. These phase plots are very different compared with the conventional phase angle curves for zero warp (Fig. 3).

2.4 Rotor Response With the Residual Bow Exactly Equal to the Unbalance Eccentricity—$\bar{\delta}_r = 1.0$. In the set of amplitude and phase angle curves represented by Figs. 14 and 15, the shaft bow is exactly equal to the rotor unbalance eccentricity.

Fig. 14 represents the rotor response curves for $\phi_r = 0$ deg (in phase response). For low speeds, considerably below the rotor critical speed, the elastic deflection of the shaft is negligible and the rotor amplitude corresponds to the residual bow of the shaft. From Fig. 14, for $f = 0$, the amplitude ratio equals 1.0. Note that critical damping is $\xi = 1.0$ and this curve is a straight line with amplitude ratio of 1.0. For all damping ratios, the amplitude ratio approaches 1.0 as $f \rightarrow \infty$. This implies that the mass center lies along the axis of rotation which has been true in all previous discussed cases. The maximum amplitude ratio is 10.0 for $\xi = 0.1$. This is about twice the value for the zero warp case. Since the residual bow is in-phase with the unbalance eccentricity, both effects combine to increase the response.

Table 4 represents critical and maximum values of amplification factors and phase angles for $\bar{\delta}_r = 1.0$ and $\phi_r = 0$ deg. Note that for all damping ratios $A_{cr} = A_{\max}$ and $\phi_{cr} = \phi_{\max}$. In fact, this is true for all ϕ_r values with $\bar{\delta}_r = 1.0$.

Table 3 Critical and maximum values of amplification factors and phase angles for various damping ratios ($\bar{\delta}_r = 2.0$, $\phi_r = 180$ deg)

$\bar{\delta}_r = 2.00$ $\phi_r = 180.0°$

ξ	A_{cr}	$A_{\max}$	ϕ_{cr}	$\phi_{\max}$	$f_{\max}$
.10	5.000	5.222	270.00	253.13	.9701
.15	3.333	3.662	270.00	245.23	.9332
.20	2.500	2.932	270.00	237.79	.8814
.30	1.667	2.291	270.00	224.00	.7365
.40	1.250	2.059	270.00	209.88	.5222
.50	1.000	2.000	270.00	180.00	0.0
.75	.667	2.000	270.00	180.00	0.0
1.00	.500	2.000	270.00	180.00	0.0
4.00	.125	2.000	270.00	180.00	0.0

Fig. 15 represents the rotor response curves for $\bar{\delta}_r = 1.0$ and $\phi_r = 180$ deg (out of phase response). Since the unbalance eccentricity equals the residual bow ($\bar{\delta}_r = 1.0$) and leads the residual bow by 180 deg ($\phi_r = 180$ deg), the two unbalances cancel each other. This is indeed the case as can be seen from Fig. 15. The amplitude ratio has a maximum value of 1.0 at $f = 0.0$ and as $f \rightarrow \infty$ for all damping ratios. The amplitude ratio is zero at $f = 1.0$ (square root of $\bar{\delta}_r = 1.0$). These response curves represent the balance rotor.

For more amplitude and phase plots considering different ϕ_r values than shown here, see Gunter, Nicholas, and Allaire [10].

3 Discussion and Conclusions—Part 1

It can be seen from the examination of the various rotor amplitude and phase plots presented for the different combinations of residual shaft bow and rotor unbalance that the dynamical response is not the same as that encountered with the conventional unbowed shaft. The effect of the residual bow causes a considerable difference in the rotor amplitude and phase angle relationships that would normally be expected with the unbowed shaft.

One important difference is that the rotor phase angle change from zero speed to the speed at which the maximum amplitude occurs is usually not 90 deg. Many people have used the 90 deg phase shift method at the critical speed as a means of determining where to place a balance weight. With a bowed shaft, this method may be considerably in error.

If the shaft bow is 180 deg out of phase with the disk unbalance, there will always be a speed at which the rotor amplitude will go to zero (equal to $\sqrt{\bar{\delta}_r}$). Whenever the amplitude goes to zero, an abrupt 180 deg phase shift occurs at $f = \sqrt{\bar{\delta}_r}$. This shift is due to the change in direction of the shaft center-line deflection vector $\vec{\delta}$.

Fig. 9 indicates that a very distinct minimum occurs in the amplitude plots for $\vec{\delta}_r$ "almost" out of phase with $\mathbf{e}_u$ (i.e., $\phi_r = 180$ deg ± 40 deg). Thus the relative size of the residual bow *may* be determined from examination of the response curves. If the rotor amplitude goes through a minimum below the critical speed, the residual bow is smaller than the mass unbalance. Conversely, if the rotor amplitude goes through a minimum above the critical speed, the residual bow is larger than the mass unbalance.

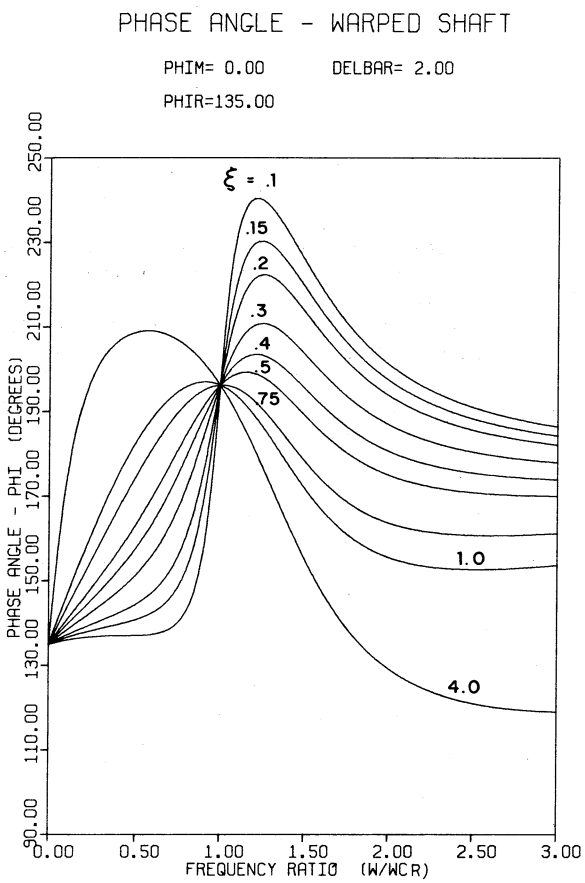

Fig. 13 Phase angle curves with $\bar{\delta}_r = 2.0$, $\phi_r = 135$ deg for various damping ratios

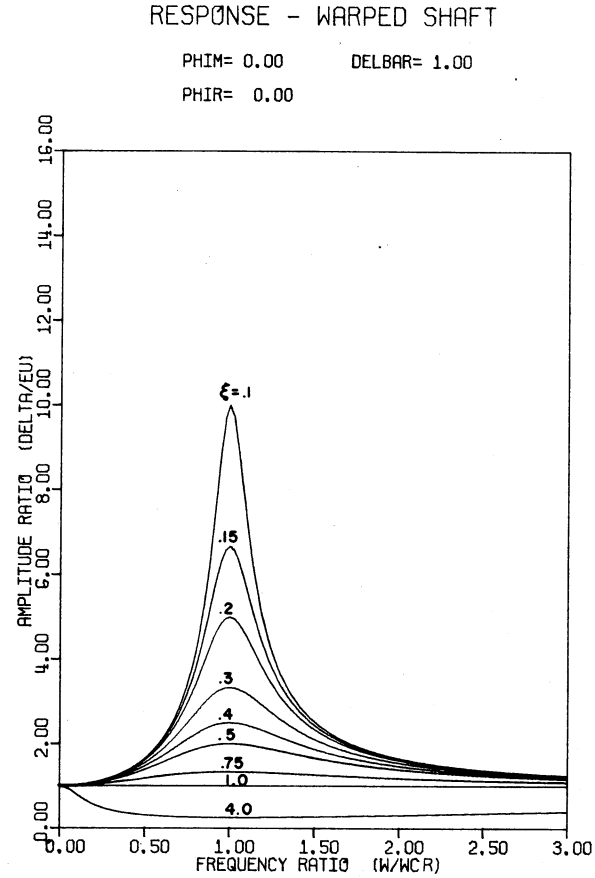

Fig. 14 Response curves with $\bar{\delta}_r = 1.0$, $\phi_r = 0$ deg for various damping ratios (in-phase response)

Table 4 Critical and maximum values of amplification factors and phase angles for various damping ratios ($\bar{\delta}_r = 1.0$, $\phi_r = 0$ deg)

$\bar{\delta}_r = 1.00$ $\phi_r = 0.0°$

ξ	A_{cr}	A_{max}	ϕ_{cr}	ϕ_{max}	f_{max}
.10	10.00	10.000	90.00	90.00	1.0000
.15	6.667	6.667	90.00	90.00	1.0000
.20	5.000	5.000	90.00	90.00	1.0000
.30	3.333	3.333	90.00	90.00	1.0000
.40	2.500	2.500	90.00	90.00	1.0000
.50	2.000	2.000	90.00	90.00	1.0000
.75	1.333	1.333	90.00	90.00	1.0000
1.00	1.000	1.000	90.00	all	all
4.00	.250	1.000	90.00	0.0	0.0

In all cases considered, the maximum amplitude occurs at a frequency above or below $f = 1.0$ except for the $\bar{\delta}_r = 1.0$ case. For $\bar{\delta}_r = 1.0$ there are no phase shifts ($\phi_{cr} = \phi_{max}$) and the maximum amplitude occurs at $f = 1.0$. For $\bar{\delta}_r = 0.5$, the maximum amplitude occurs at a frequency *above* $f = 1.0$ and the phase angle at maximum am-

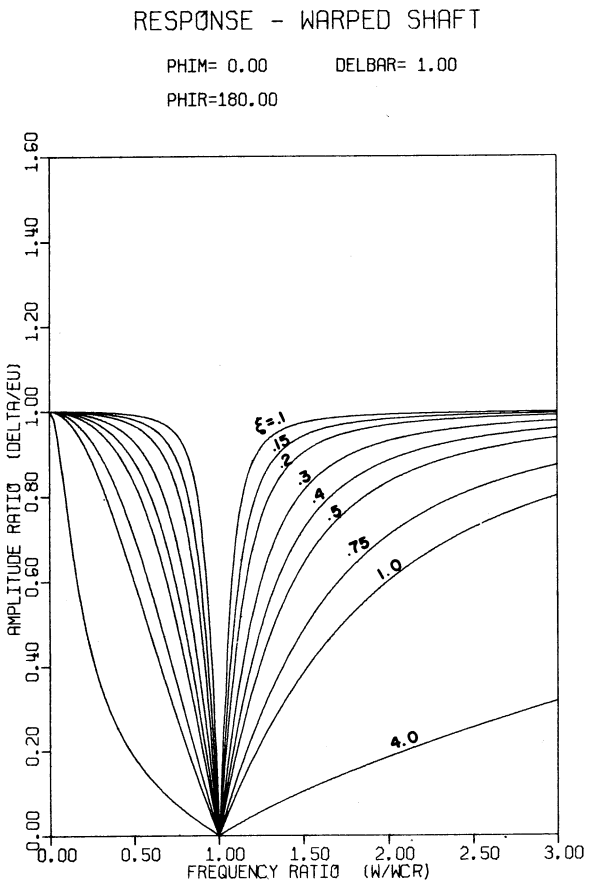

Fig. 15 Response curves with $\bar{\delta}_r = 1.0$, $\phi_r = 180$ deg for various damping ratios, balanced rotor (out of phase response)

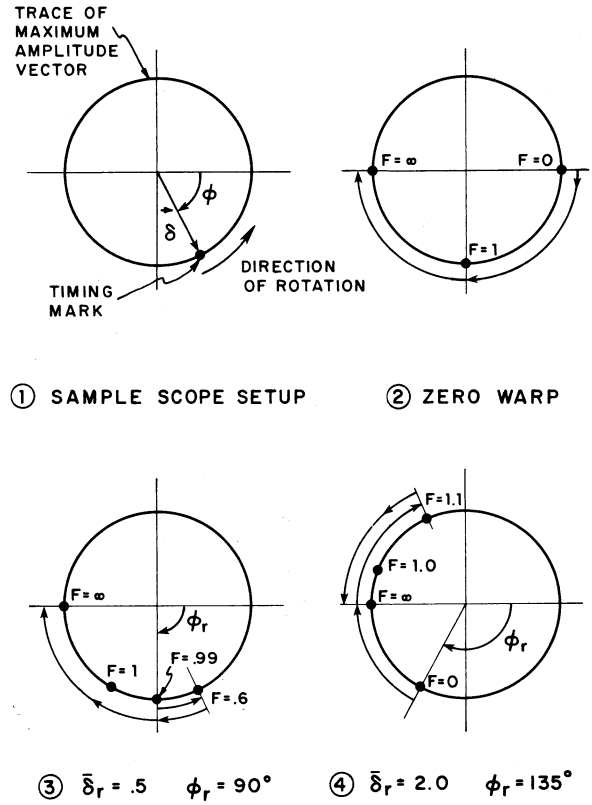

Fig. 16 Schematic showing the movement of the timing mark on an oscilloscope screen as speed increases for various $\bar{\delta}_r$ and ϕ_r values (for damping ratios below critical damping)

plitude *increases* from the ϕ_{cr} value. On the other hand, for $\bar{\delta}_r$ = 2.0, the maximum amplitude occurs at a frequency *below* f = 1.0 and the phase angle at maximum amplitude *decreases* from the ϕ_{cr} value.

Fig. 5 indicates that for low damping ratios the phase angle decreases for frequency ratios between f = 0 and f = 0.7. This does not occur for the zero warp case. Fig. 13 shows that for frequency ratios above f = 1.0, the phase angle increases to values above 180 deg before they approach 180 deg as $f \rightarrow \infty$. Again, this does not occur for the zero warp case. Fig. 16 shows how these phase angle changes may be observed on an oscilloscope. As the rotor rotates, the maximum amplitude vector is traced on the screen. When the reference timing mark on the disk lines up with the phase reference probe, a timing dot lights up on the screen at the location of $\bar{\delta}$ (see Fig. 16–1). For the zero warp case the timing mark or dot moves opposite to the direction of rotation as f increases (Fig. 16–2). For $\bar{\delta}_r$ = 0.5 and ϕ_r = 90 deg, the timing mark initially moves in the direction of rotation as f increases for speeds below f = 0.6 (see Fig. 16–3). Fig. 16–4 shows the timing mark moving opposite the direction of rotation as f increases until slightly above the critical speed where it changes direction at f = 1.1.

Fig. 16 is for the special case of ϕ_m = 0 (reference timing mark in line with the unbalance eccentricity). However, these results may be applied in general. When the shaft is perfectly straight, the timing mark moves opposite to the direction of rotation as f increases. Furthermore, if the shaft has a residual bow and the damping is less than the critical value, the following conclusions hold:

1 If the residual warp is less than the unbalance, the timing mark will first move in the direction of rotation as the speed is increased and then switch direction at a speed less than the critical speed.

2 If the residual warp is greater than the unbalance, the timing mark first moves opposite to the direction of rotation as the speed is increased. At some speed above the critical speed, the timing mark will reverse directions and begin moving in the direction of rotation for increasing speeds. Thus the relative amplitudes of the residual warp and mass unbalance may be determined simply by an observation of the direction of timing mark movement on an oscilloscope.

In an actual machine, rotor bow may be caused by many effects such as shrink fit of wheels and spacers and thermal bows due to localized rubbing or thermal gradients. Quite often the thermal bow is induced into the rotor at an operating condition due to the local rubbing of a seal. When this occurs there is usually an associated phase angle shift. Therefore a very good way to detect a thermal bow occuring during operation is by observation of the phase angle change during running. If the phase angle changes slowly with time while operating at a constant speed it may be due to a thermal bow being induced into the shaft by means of a localized rub.

By examining the response curves presented here, insight into balancing a rotor with a residual bow may be obtained. Details of balancing a bowed rotor are discussed in Part II.

References

1 Newkirk, B. L., "Shaft Rubbing," *Mechanical Engineering*, Vol. 48, 1926, p. 830.

2 Dimarogonas, A. D., "An Analytic Study of the Packing Rub Effect in Rotating Machinery," Dissertation, Rensselaer Polytechnic Institute, Troy, New York, 1970.

3 Kikuchi, K., "Analysis of Unbalance Vibration of Rotating Shaft System With Many Bearings and Disks," *Bull J.S.M.E.*, Vol. 13, No. 61, 1970.

4 Yamamoto, T., "On the Critical Speeds of a Shaft," Memoirs of the Faculty of Engineering, Nagoya University, Japan, Nov., 1954.

5 Sternlicht, B., and Lewis, P., "Vibration Problems With High-Speed Turbomachinery," *Journal of Engineering for Ind.*, TRANS. ASME, Feb. 1968.

6 Jeffcott, H. H., "The Lateral Vibration of Loaded Shafts in the

Neighborhood of a Whirling Speed . . . the Effect of Want of Balance," *Phil. Mag.*, Series 6, Vol. 37, 1919.

7 Thompson, W. T., *Theory of Vibration With Applications*, Prentice Hall, New Jersey, 1972.

8 Myklestad, N. O., *Fundamentals of Vibration Analysis*, McGraw-Hill, New York, 1956.

9 Gunter, E. J., "Dynamic Stability of Rotor-Bearing Systems," NASA SP-113 Office of Technical Information, Washington, D. C., 1966.

10 Gunter, E. J. Nicholas, J. C., and Allaire, P. E., "Effect of Residual Shaft Bow on Dynamic Respone and Balancing of Single Mass Rotors," Report No. ME-543-103-74, Department of Mechanical Engineering, University of Virginia, Charlottesville, Va., Jan. 1974.

Reprinted from ENGINEERING FOR POWER, *Vol. 98, No. 2, April 1976*

J. C. Nicholas
Research Associate.

E. J. Gunter
Assoc. Professor.

P. E. Allaire
Assist. Professor.

University of Virginia,
Charlottesville, Va.

Effect of Residual Shaft Bow on Unbalance Response and Balancing of a Single Mass Flexible Rotor

Part II: Balancing

Three methods of balancing a rotor with a residual shaft bow were presented. Method I balanced the total shaft amplitude to zero at the balance speed. Method II balanced the elastic deflection to zero at the balance speed leaving the residual bow amplitude. Method III balanced the total shaft amplitude to zero at the critical speed without actually operating the rotor at the critical. After balancing by Method I, a large amplitude remained near the critical. Method II balanced the rotor to the residual bow amplitude at all speeds except near the critical where the amplitude is slightly larger than the residual amplitude. The optimum balance resulted from balancing by Method III. In this case, the amplitude was less than or equal to the residual bow amplitude for all speeds except at the critical where the amplitude was zero. Method III required that the critical speed be known prior to balancing. For all three balancing methods, the unbalance influence coefficient must be determined. Two procedures for determining this coefficient were discussed. One was the familiar trial weight influence coefficient method and the other was the direct method which does not require trial weights. Part I of this paper discussed the effect of shaft bow on unbalance response.

Introduction

Vibration levels in rotating machinery are usually affected by both shaft flexibility and residual bow. Bishop [1][1] gave an elementary explanation of the difference between balancing for mass unbalance and for residual bow. It was shown that an initially bent rotor without mass unbalance could be balanced so that zero vibration resulted at the critical speed.

A general modal method for balancing a flexible shaft with both mass unbalance and residual shaft bow has been discussed by Bishop and Gladwell [2] and applied to a uniform shaft. Parkinson, Jackson, and Bishop [3] theoretically showed that the optimum balance weight should be chosen so that the vector sum of unbalance eccentricity, residual bow, and balance eccentricity be zero. In the second part of this paper [4], they demonstrated experimentally that a shaft with residual bow but no mass unbalance could be balanced to nearly zero vibration at the critical speed.

The balancing of industrial rotors is carried out primarily by the influence coefficient method [5]. Refinements such as applying least squares error criteria [6], taking into account shaft flexibility [7, 8, 9, 10] and discussion of the effect of rigid body balancing [11, 12] have emerged in recent years. Wilcox [13] discusses the balancing of a bowed uniform shaft. However, no study of the effect of residual shaft bow on the influence coefficient method for flexible rotors has been carried out.

It is usually not possible to balance a rotor with the influence coefficient method at a critical speed [14] due to the large amplitudes of vibration and difficulties of maintaining constant operating speed there. In spite of this, the optimum balancing speed is the critical speed. Thus it is desirable to develop a method which would allow balancing at an off critical speed resulting in optimum balancing at the critical speed. If a change in unbalance occurs due to erosion or other factors, the vibration level at an operating speed near a critical will be minimized.

Although the analysis presented here is for a single mass Jeffcott type rotor, the results may be extended to a multimass rotor operating below the second critical speed. The simple model provides

[1] Numbers in brackets designate References at end of paper.

Contributed by the Gas Turbine Division and presented at the Gas Turbine Conference, Houston, Texas, March 2–6, 1975, of THE AMERICAN SOCIETY OF MECHANICAL ENGINEERS. Manuscript received at ASME Headquarters December 2, 1974. Paper No. 75-GT-49.

an approximate balancing procedure which may utilize the first critical speed obtained from the widely available critical speed programs.

Part I of this paper discussed the theoretical unbalance response analysis of a single mass rotor with a residual shaft bow. Part II is concerned with a discussion of the balancing of this rotor.

4 Balancing a Single Mass Rotor With a Bowed Shaft

4.1 Theoretical Development. The balancing of a flexible rotor with unbalance plus residual bow is normally carried out by the influence coefficient method [5]. Total rotor response may be considered as composed of the sum of the responses due to disk unbalance and shaft bow as follows,

$$Z = \alpha_u \hat{e}_u + \alpha_r \hat{\delta}_r \tag{26}$$

where α_u and α_r are the complex influence coefficients for the disk unbalance and shaft residual bow, respectively. Z is the complex amplitude of motion. The values $\hat{e}_u$ and $\hat{\delta}_r$ are also complex (unbalance and residual bow, respectively). Both of the influence coefficients are usually evaluated experimentally for a particular rotor but equation (9) gives the values associated with the single mass rotor analyzed in Section I as

$$\alpha_u = \frac{m\omega^2}{k - m\omega^2 + ic\omega} \tag{27}$$

$$\alpha_r = \frac{k}{k - m\omega^2 + ic\omega} \tag{28}$$

Note that both influence coefficients vary with the rotor speed at which they are evaluated. Three balancing procedures are illustrated here by considering their effect on the response of the single mass model. The three balancing procedures are

I Balancing the total shaft deflection to zero at the balance speed.

II Balancing to minimize the elastic shaft deflection at the balance speed.

III Balancing the total shaft deflection to zero at the critical speed without actually operating at the critical.

Method I seems to be suggested by Figs. 6 and 11 where the total shaft deflection is zero for a speed below and above the critical speed respectively. These two cases clearly show that large amplitudes remain near the critical speed indicating that Method I is not the optimum balancing procedure.

With this knowledge, Method II is suggested. In this case, the elastic deflection is brought to zero at the balance speed leaving the residual displacement.

Examination of Fig. 15 suggests that if the total shaft deflection is brought to zero at the critical then the rotor is balanced at all speeds (i.e., the response is less than or equal to the residual deflection at all speeds). This may be accomplished by Method I if the balance speed ω_b is equal to the critical speed ω_{cr}. However, Parkinson, et al. [3] shows how this may be done at any balance speed. This is Method III and appears to be the optimum balance.

4.2 Discussion of Balancing Methods.

Method I. Consider Z_1 as the complex amplitude of motion at the balance speed ω_b before balancing. From equation (26)

$$Z_1 = \alpha_u \hat{e}_u + \alpha_r \hat{\delta}_r$$

This may be rewritten as

$$Z_1 = \alpha_u \left(\hat{e}_u + \frac{\alpha_r}{\alpha_u} \hat{\delta}_r\right) \tag{29}$$

Let the equivalent unbalance eccentricity $\hat{e}_u'$ be

$$\hat{e}_u' = \hat{e}_u + \frac{\alpha_r}{\alpha_u} \hat{\delta}_r \tag{30}$$

Thus

$$\hat{e}_u' = \frac{Z_1}{\alpha_u} \tag{31}$$

Choose the balance eccentricity $\hat{e}_b$ (complex) such that

$$\hat{e}_b = -\hat{e}_u' \tag{32}$$

Or

$$\hat{e}_b = -\frac{Z_1}{\alpha_u} \tag{33}$$

Note that Z_1 may be determined experimentally by running at the balance speed ω_b. Also, α_u may be calculated by one of two methods discussed in Section 4.3. With these two values known, the balance eccentricity may be determined from equation (33). The balance weight is determined by

$$U_b = |\hat{e}_b| \times W \qquad \text{N-cm (oz-in.)} \tag{34}$$

where W is the weight in newtons (pounds) of the rotor. The location of the balance weight is given by the angle of $\hat{e}_b$. Let Z_2 be the complex amplitude of motion at ω_b after the balancing weight given by equation (34) has been added. Thus

$$Z_2 = \alpha_u (\hat{e}_u + \hat{e}_b) + \alpha_r \hat{\delta}_r \tag{35}$$

Substituting equations (30) and (32) into equation (35) yields

$$Z_2 = \alpha_u \left(\hat{e}_u - \hat{e}_u - \frac{\alpha_r}{\alpha_u} \hat{\delta}_r\right) + \alpha_r \hat{\delta}_r$$

Or

$$Z_2 = 0$$

Thus, the total shaft deflection is zero at ω_b after balancing. This is balancing procedure I.

Method II. Return to equation (26) with Z_1 as the complex amplitude of motion at ω_b before balancing

$$Z_1 = \alpha_u \hat{e}_u + \alpha_r \hat{\delta}_r$$

If the shaft stiffness, k, is large compared to the amplitude of the mass and damping terms in equation (28), the residual bow influ-

Nomenclature

c = shaft dampling, N-s/cm (lb-s/in.)
$\mathbf{e}_u$ = unbalance eccentricity vector
$\hat{e}_u$ = complex unbalance eccentricity
e_u = unbalance eccentricity, $|\mathbf{e}_u|$, cm (in.)
$\hat{e}_u'$ = complex equivalent unbalance eccentricity
$\hat{e}_b$ = complex balance eccentricity
$\hat{e}_t$ = complex trial weight eccentricity
f = frequency ratio, ω/ω_{cr}, dim
f_{cr} = critical frequency ratio, dim
k = shaft spring rate, N/cm (lb/in.)
m = rotor mass, N-s²/cm (lb-s²/in.)
U_b = balance weight, N-cm (oz-in.)
U_t = trial weight, N-cm (oz-in.)
W = rotor weight, N (lb)
Z = complex shaft amplitude
Z_t = complex shaft amplitude due to the addition of a trial weight
Z_{cr} = complex shaft amplitude measured at the critical speed
α_r = complex shaft residual bow influence coefficient, dim
α_u = complex unbalance influence coefficient, dim
$\vec{\delta_r}$ = residual bow vector
$\hat{\delta}_r$ = complex residual bow
$\vec{\delta_r}$ = residual bow, $|\vec{\delta}|$, cm (in.)
$\vec{\delta}$ = shaft center-line deflection vector
ϕ = phase angle between the shaft center-line vector $\vec{\delta}$ and the shaft reference timing mark
ϕ_{cr} = phase angle ϕ at rotor critical speed
ϕ_m = angle between mass center and shaft reference timing mark
ϕ_r = angle between residual bow vector $\vec{\delta_r}$ and the shaft reference timing mark
ω = shaft angular velocity, rad/s
ω_b = balance speed, rad/s
ω_{cr} = rotor critical speed $\sqrt{k/m}$, rad/s

ence coefficient, α_r may be taken as unity. Then the residual bow may be subtracted from the rotor amplitude.

$$Z_1 - \hat{\delta}_r = \alpha_u \hat{e}_u \tag{36}$$

Thus,

$$\hat{e}_u = \frac{Z_1 - \hat{\delta}_r}{\alpha_u} \tag{37}$$

Choose the balance eccentricity $\hat{e}_b$ such that

$$\hat{e}_b = -\hat{e}_u$$

Or

$$\hat{e}_b = -\frac{Z_1 - \hat{\delta}_r}{\alpha_u} \tag{38}$$

This is the balance eccentricity prescribed by Method II. As in Method I, Z_1 is measured experimentally at ω_b and α_u determined by the methods described in Section 4.3. The amount and phase angle of $\hat{\delta}_r$ may also be determined experimentally by running the rotor at a very low speed. From the plots presented in Section II, it is clear that at low speeds the shaft amplitude equals the residual bow and the phase angle is ϕ_r (angle by which the reference timing mark leads $\hat{\delta}_r$).

Method II balances the rotor down to the residual bow at the balance speed ω_b (i.e., the elastic shaft deflection is brought to zero at ω_b). The method assumes that the residual bow does not change with rotor speed when, in fact, equation (28) shows that α_r does depend on speed. It will be shown in Section 4.4 that balancing at ω_b using Method II leaves a small amplitude (slightly larger than the residual bow) near the critical. However, the method is much better than Method I.

Method III. Clearly, the optimum balance is given by Fig. 15. This may be accomplished by Method I with the disadvantage that the rotor must be operated unbalanced at the critical. Method III balances the rotor to zero total amplitude at the critical without actually operating the rotor at ω_{cr}.

If a balance weight with eccentricity $\hat{e}_b$ is added to the rotor, then the amplitude response is given by

$$Z_2 = \alpha_u(\hat{e}_u + \hat{e}_b) + \alpha_r \hat{\delta}_r \tag{39}$$

Substituting for α_u and α_r using equations (27) and (28) yields

$$Z_2 = \frac{1}{k - m\omega^2 + ic\omega}[m\omega^2(\hat{e}_u + \hat{e}_b) + k\hat{\delta}_r]$$

It is desired that the rotor amplitude be zero at the critical speed such as shown in Fig. 15.

$$Z_2\big|_{\omega=\omega_{cr}} = 0$$

Since $k = m\omega_{cr}^2$, the balance criterion reduces to

$$\hat{e}_u + \hat{e}_b + \hat{\delta}_r = 0$$

Or

$$\hat{e}_b = -(\hat{e}_u + \hat{\delta}_r) \tag{40}$$

Where $\hat{\delta}_r$ may be determined from the residual runout.

To determine $\hat{e}_u$, consider the ratio of α_r/α_u. From equations (27) and (28) with

$$\alpha_r/\alpha_u = \frac{k}{m\omega_b^2}$$

or

$$\alpha_r = (\frac{\omega_{cr}}{\omega_b})^2 \alpha_u \tag{41}$$

If the critical speed is known then α_r can be calculated (α_u determined by methods of Section 4.3).

The amplitude of motion at the balance speed ω_b before balancing is given by

$$Z_1 = \alpha_u \hat{e}_u + \alpha_r \hat{\delta}_r$$

With α_r known, $\hat{e}_u$ can be calculated.

$$\hat{e}_u = \frac{Z_1 - \alpha_r \hat{\delta}_r}{\alpha_u}$$

$$\hat{e}_u = \frac{Z_1}{\alpha_u} - (\frac{\omega_{cr}}{\omega_b})^2 \hat{\delta}_r \tag{42}$$

Thus, $\hat{e}_b$ can be calculated using equations (40) and (42) and the rotor balanced to zero at the critical speed without actually operating the rotor at ω_{cr}. The only disadvantage is that ω_{cr} must be known. From equations (40) and (42), the balance eccentricity is given by

$$\begin{aligned} \hat{e}_b &= -\frac{Z_1}{\alpha_u} + (\frac{\alpha_r}{\alpha_u} - 1)\hat{\delta}_r \\ \hat{e}_b &= -\frac{Z_1}{\alpha_u} + \frac{\omega_{cr}^2 - \omega_b^2}{\omega_b^2}\hat{\delta}_r \end{aligned} \tag{43}$$

4.3 Determination of the Unbalance Influence Coefficient, α_u. All three balancing methods discussed in Section 4.2 require prior calculation of the unbalance influence coefficient, α_u. There are two basic methods by which α_u can be determined. The first method is the familiar influence coefficient method in which a trial weight is added to the disk. This method will be called the influence coefficient trial weight method. The second method employs direct measurement of the rotor amplitude and phase angles at various speeds without the addition of a trial weight. This method will be called the direct method.

The influence coefficient trial weight method discussed by Thearle [5] will be reviewed briefly. The amplitude of motion at the balance speed is given by

$$Z_1 = \alpha_u \hat{e}_u + \alpha_r \hat{\delta}_r$$

After a trial weight U_t has been added, (which yields a trial weight eccentricity $\hat{e}_t$) the amplitude at the balance speed is

$$Z_t = \alpha_u(\hat{e}_u + \hat{e}_t) + \alpha_r \hat{\delta}_r \tag{44}$$

Subtracting

$$Z_t - Z_1 = \alpha_u \hat{e}_t$$

or

$$\alpha_u = \frac{Z_t - Z_1}{\hat{e}_t} \tag{45}$$

Thus, α_u can be calculated since $\hat{e}_t$ is known while Z_1 and Z_t are measured experimentally.

The direct method assumes that the rotor mass is known. If the rotor is run at three different speeds without the use of trial weights, the amplitudes at these three speeds are

$$\begin{aligned} Z_1 &= \alpha_u \hat{e}_u + \alpha_r \hat{\delta}_r, \quad \omega = \omega_1 \\ Z_2 &= \alpha_u \hat{e}_u + \alpha_r \hat{\delta}_r, \quad \omega = \omega_2 \\ Z_3 &= \alpha_u \hat{e}_u + \alpha_r \hat{\delta}_r, \quad \omega = \omega_3 \end{aligned} \tag{46}$$

The amplitudes are measured experimentally at each speed. Using equations (27) and (28), equations (46) can be written in matrix form. The three unknowns are $\hat{e}_u$, the effective shaft stiffness k, and the effective damping c.

$$\begin{Bmatrix} \hat{e}_u \\ k \\ c \end{Bmatrix} = -m \begin{bmatrix} m\omega_1^2 & \hat{\delta}_r - Z_1 & i\omega_1 Z_1 \\ m\omega_2^2 & \hat{\delta}_r - Z_2 & i\omega_2 Z_2 \\ m\omega_3^2 & \hat{\delta}_r - Z_3 & i\omega_3 Z_3 \end{bmatrix}^{-1} \begin{Bmatrix} Z_1\omega_1^2 \\ Z_2\omega_2^2 \\ Z_3\omega_3^2 \end{Bmatrix} \tag{47}$$

If the critical speed is also known, and since it has already been assumed that m is known, k can be solved for immediately. Thus only two equations are necessary to solve for the two unknowns $\hat{e}_u$ and c. Using equations (27) and (28), α_u and α_r may be calculated since k and c can be determined from equation (47).

4.4 Example Balance Calculations. Given:

$$W = 16.9\,\text{N} \quad (3.8\ \text{lb}) \tag{48}$$

$$k = 817.8\,\text{N/cm} \quad (467\ \text{lb/in.}) \tag{49}$$

$$c = 0.385\,\text{N-s/cm} \quad (.22\ \text{lb-s/in.}) \tag{50}$$

The disk is assumed to have an unbalance eccentricity of $e_u = 2.54$

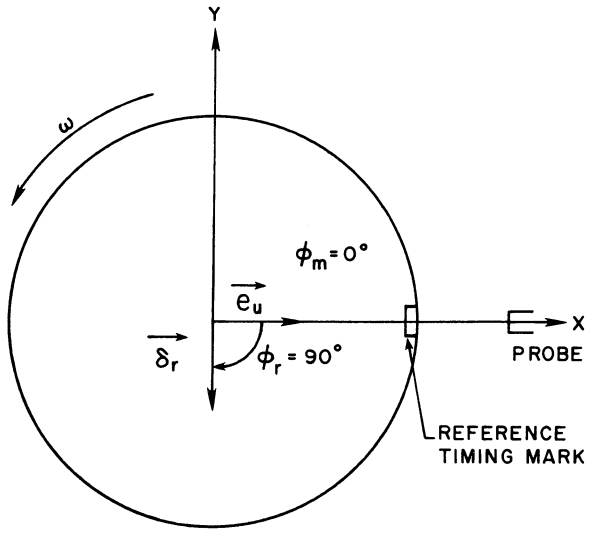

Fig. 17 Rotor schematic for sample balance problem

$\times 10^{-3}$ cm (1 mil) at a phase location of $\phi_m = 0$ deg (unbalance eccentricity in line with the reference timing mark). Also, the residual bow has a magnitude of $\delta_r = 2.54 \times 10^{-3}$ cm (1 mil) at the phase angle position of $\phi_r = 90$ deg (reference timing mark leads the residual bow vector by 90 deg). See Fig. 17 for a schematic. Thus

$$\hat{e}_u = 2.54 \times 10^{-3} e^{i360°} \text{cm} \ (1.0\, e^{i360°} \text{ mils}) \quad (51)$$

$$\hat{\delta}_r = 2.54 \times 10^{-3} e^{-i90°} \text{cm} \ (1.0\, e^{-i90°} \text{ mils}) \quad (52)$$

Consider the balance speed to be $\omega_b = 188.5$ rad/s (1800 rpm). The critical speed is $\omega_{cr} = 217.9$ rad/s (2081 rpm). The influence coefficients may be calculated directly from equations (27) and (28) using $\omega = \omega_b$

$$\alpha_u = 2.79\, e^{-i19.4°}$$

$$\alpha_r = 3.77\, e^{-i19.4°} \quad (53)$$

The amplitude at ω_b may be determined from equation (26)

$$Z_1 = \alpha_u \hat{e}_u + \alpha_r \hat{\delta}_r \quad (54)$$

Using equations (51), (52), (53), and (54), Z_1 can be calculated. In-

$$Z_1 = 11.9 \times 10^{-3} e^{-i72.9°} \text{cm} \ (4.69\, e^{-i72.9°} \text{mils}) \quad (55)$$

Normally, most of the quantities given in equations (48), (49), (50), (51), and (52) will not be known. However, they are specified here so that Z_1 may be calculated. Z_1 is usually determined experimentally by operating the rotor at ω_b (1800 rpm). Also, α_u will normally be calculated using the influence coefficient trial weight method outlined in Section 4.3. This method requires that a known trial weight be added. Pick a trial weight such that the trial weight eccentricity is

$$\hat{e}_t = 2.54 \times 10^{-3} e^{i360°} \text{cm} \ (1.0\, e^{i360°} \text{mils})$$

Equation (44) yields

$$Z_2 = 17.1 \times 10^{-3} e^{-i53.5°} \text{cm} \ (6.73\, e^{-i53.5°} \text{mils})$$

Again, Z_2 is normally determined experimentally by operating the rotor at ω_b with the trial weight. Equation (45) yields

$$\alpha_u = 2.79\, e^{-i19.4°} \quad (56)$$

as in equation (53).

Now that α_u has been determined, the three balancing methods discussed in Section 4.2 will be used to balance the rotor.

Method I. Method I balances the total shaft deflection to zero at the balance speed. Equation (33)

$$\hat{e}_b = -\frac{Z_1}{\alpha_u}$$

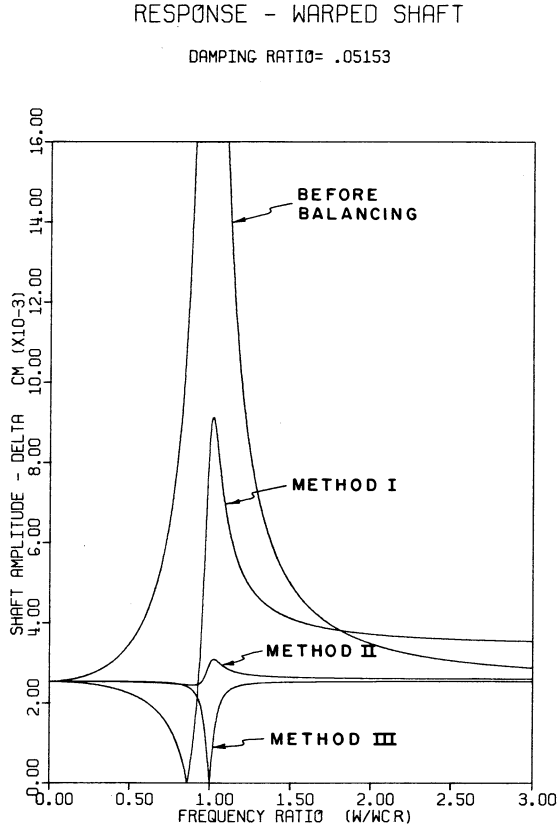

Fig. 18 Response curves before and after balancing a bowed shaft by balancing Methods I, II, and III

With equations (55) and (56), the balance eccentricity is

$$\hat{e}_b = 4.27 \times 10^{-3} e^{i126.5°} (1.68\, e^{i126.5°} \text{mils}) \quad (57)$$

The amplitude at the critical speed after balancing is given by

$$Z_{cr} = [\alpha_u(\hat{e}_u + \hat{e}_b) + \alpha_r \hat{\delta}_r]_{\omega=\omega_{cr}} \quad (58)$$

At the critical speed, $\alpha_u = \alpha_r$. From equation (27) with $\omega = \omega_{cr} = \sqrt{k/m}$

$$\alpha_u = \alpha_r = \frac{m\omega_{cr}}{ic} \quad (59)$$

Therefore

$$\alpha_u = \alpha_r = 9.74\, e^{-i90°}$$

With equations (51), (52), and (57)

$$Z_{cr} = 8.66 \times 10^{-3} e^{i360°} \text{cm} \ (3.41\, e^{i360°} \text{mils}) \quad (60)$$

Thus the rotor amplitude after balancing to zero at ω_b is 8.66×10^{-3} cm (3.41 mils) at the critical speed.

Figs. 18 and 19 show the response and phase angle curves for the rotor given in this example. The response curve for the unbalanced rotor is indicated in Fig. 18. Note that for $f_b = \omega_b/\omega_{cr} = 0.86$, the amplitude is 11.9×10^{-3} cm as in equation (55). Fig. 19 shows a phase of about $\phi = 75$ deg for the unbalanced case at $f_b = 0.86$. This is very close to the phase angle indicated in equation (55).

After balancing by Method I, the response curve as shown by Fig. 18 is similar to Fig. 6 and Fig. 11 (i.e., rotor balanced to zero at ω_b and a large amplitude remaining near the critical). Note that the amplitude at a frequency ratio of 1.0 ($\omega = \omega_{cr}$) is approximately 8.6×10^{-3} cm as in equation (60). Also, close examination of Fig. 18 shows that the maximum amplitude of about 9.1×10^{-3} cm occurs at a frequency ratio slightly higher than 1.0.

The phase plot after balancing by Method I is shown in Fig. 19. Note the 180 deg phase shift that occurs at f_b. This is expected

since the amplitude is zero at f_b. The same type of 180 deg shift occurs in Figs. 7 and 12 for the reasons discussed in Section 2.2. The phase shift that occurs at $f = 1.0$ is mathematical rather than physical (i.e., a 360 deg shift). Fig. 19 indicates a phase angle of $\phi_{cr} = 0$ deg or 360 at $f = 1.0$. This agrees with equation (60).

Method II. Method II balances to minimize the elastic shaft deflection at the balance speed. The balance eccentricity may be determined from equation (38).

$$\hat{e}_b = -\frac{Z_1 - \hat{\delta}_r}{\alpha_u}$$

Using equations (52), (53), and (55), $\hat{e}_b$ can be determined.

$$\hat{e}_b = 3.4 \times 10^{-3} e^{i131^\circ} \text{cm} \ (1.34 e^{i131^\circ} \text{mils}) \qquad (61)$$

The amplitude at the critical speed after balancing by Method II is

$$Z_{cr} = 2.99 \times 10^{-3} e^{-i84.2^\circ} \text{cm} \ (1.18 e^{-i84.2^\circ} \text{mils}) \qquad (62)$$

The result of balancing the given rotor using Method II is also shown in Figs. 18 and 19. Fig. 18 shows a response curve that is almost a straight line except for a slight bump at f_{cr}. The amplitude at speeds everywhere except near the critical equals δ_r. Note that the elastic deflection is zero for all speeds except near the critical.

Fig. 19 shows the phase plot for Method II. It is also a straight line with a slight downward bump near f_{cr}. At all frequency ratios except near f_{cr}, the phase angle $\phi = 90$ deg which is ϕ_r.

Method III. Method III balances the total shaft deflection to zero at the critical speed. First, α_r must be calculated (assuming ω_{cr} known) using equation (41)

$$\alpha_r = \left(\frac{\omega_{cr}}{\omega_b}\right)^2 \alpha_u$$

With α_u given by equation (56)

$$\alpha_r = 3.73 e^{-i19.4^\circ} \qquad (63)$$

The balance eccentricity is given by equation (43)

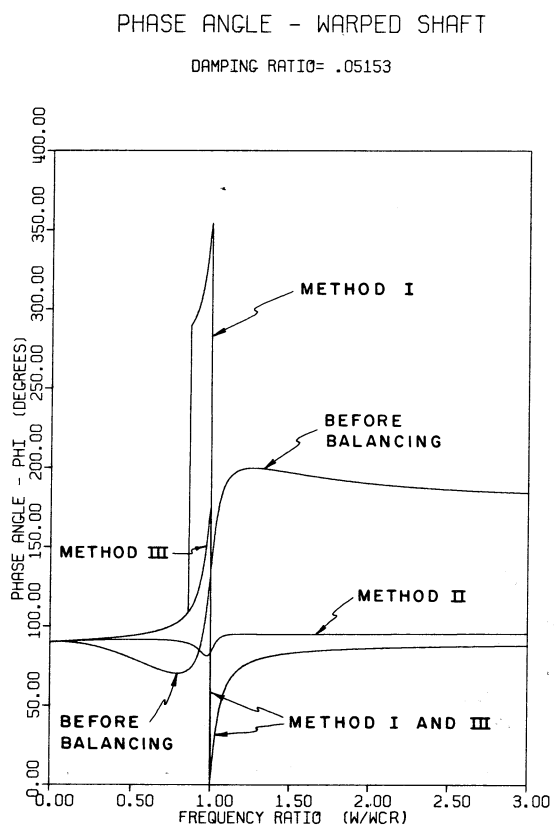

Fig. 19 Phase angle curves before and after balancing a bowed shaft by balancing Methods I, II, and III

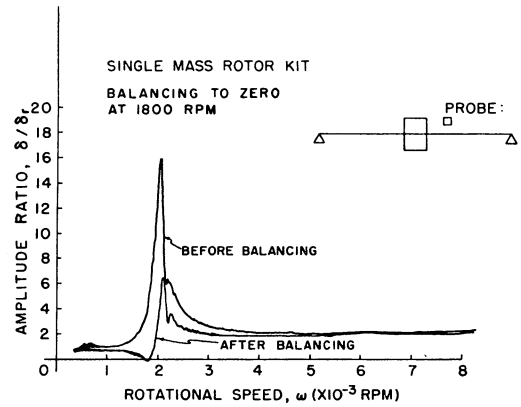

Fig. 20 Experimental response curves before and after balancing to zero at 2050 rpm

$$\hat{e}_b = \hat{\delta}_r \left(\frac{\alpha_r}{\alpha_u} - 1\right) - \frac{Z_1}{\alpha_u}$$

Using equations (52), (55), (56), and (63)

$$\hat{e}_b = 3.59 \times 10^{-3} e^{i135^\circ} \text{cm} \ (1.41 e^{i135^\circ} \text{mils}) \qquad (64)$$

Fig. 18 shows the response curve for balancing by Method III. As expected, this is the optimum balance as in Fig. 15. Fig. 19 shows the phase angle curve for Method III. Note the 180 deg phase shift at $f = 1.0$. This shift occurs since the amplitude goes to zero at $f = 1.0$ (see Section 2.2).

Similar experimental and theoretical response curves for a uniform, flexible shaft corresponding to balancing Method I and III of Fig. 18 are shown in Parkinson, et al. [3, 4].

5 Experimental Balancing Results

5.1 Experimental Equipment. A flexible single mass rotor mounted in plain journal bearings was used to evaluate the effect of rotor bow on the dynamics and balancing of the rotor. The test rig consisted of a 17.79 N (4.0 lb) disk mounted midway between the bearings. The bearing span was 30.48 cm (12.0 in.) and the shaft diameter was 0.9525 cm (0.375 in.). The bearing stiffness and damping were estimated to be 1576.1 N/cm (900 lb/in.) and 0.35 N-s/cm (0.2 lb − s/in.) for each bearing. Bently noncontacting probes were used to measure amplitude at the rotor center and to establish a phase reference signal. The results were observed both on an oscilloscope and a Bently vector tracking filter. The amplitude was plotted on an x-y plotter.

5.2 Experimental Techniques. The amplitude and phase of the residual bow, $\hat{\delta}_r$, were measured at low speed. The balancing speed ω_b was chosen to be 1800 rpm which was below the rotor critical speed. The rotor was run at ω_b and the shaft amplitude and phase, Z_1, were measured. A known trial weight was then placed on the disk and the amplitude and phase, Z_t, were again measured at ω_b. The unbalance influence coefficient, α_u, was then calculated using equation (45). The rotor was balanced twice using the methods discussed in Section 4.2. First, the rotor was balanced to zero amplitude at ω_b. Then, the rotor was balanced to zero amplitude at the critical speed.

5.3 Results. Fig. 20 shows the experimental response curves for the rotor before balancing and after balancing to zero amplitude at 1800 rpm. Note that for the "after balancing" curve, a large amplitude remains near the critical speed as predicted by balancing Method I of Section 4.2. This curve is very similar to the response curves of Fig. 6. It also matches the response curve of Fig. 18 for balancing by Method I.

The experimental curves of Fig. 21 represent the rotor response before balancing and after balancing to zero amplitude at the critical speed. The "after balancing" curve corresponds very closely to

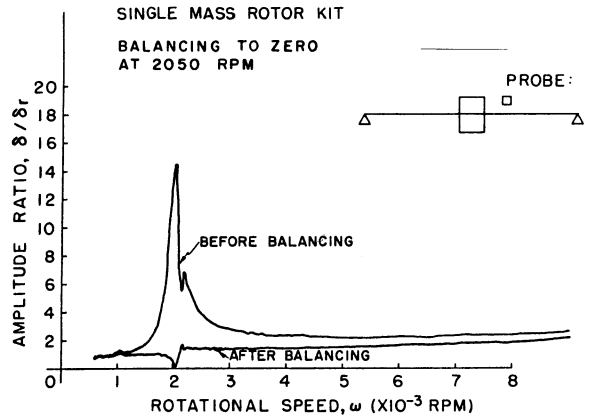

Fig. 21 Experimental response curves before and after balancing to zero at 1800 rpm

Fig. 15 (i.e., the optimum balance). It also is very similar to the response curve of Fig. 18 for balancing Method III.

6 Discussion and Conclusions—Part II

The optimum balance of a rotor with a bowed shaft results in the shaft amplitude being less than or equal to the residual bow for all speeds and equal to zero at the critical. This optimum balance is achieved by balancing the rotor to zero amplitude at ω_{cr}. Balancing Method I results in the optimum case only when $\omega_b = \omega_{cr}$. This requires the rotor to be operated unbalanced at the critical. Method III produces the optimum balance without actually operating the rotor at ω_{cr}. However, the critical speed must be known prior to balancing.

Balancing by Method I with ω_b not equal to ω_{cr} reduces the shaft amplitude to zero at ω_b. However, large amplitudes remain near the critical.

Method II balances the elastic deflection to zero at ω_b leaving the residual bow amplitude. This procedure results in amplitudes equal to the residual bow for all speeds except near the critical where the amplitude is slightly larger then δ_r.

Clearly Method III is the best balancing procedure discussed in Section 4.2. If the critical speed is not known, a combination of Methods I and II may be employed. First, balance the rotor using Method II. Method I may then be used with $\omega_b = \omega_{cr}$ to balance the shaft amplitude to zero at ω_{cr}. In this case, operating the rotor at ω_{cr} will not be so undesirable since the amplitude at ω_{cr} has been reduced considerably by the first balance of Method II. This combination balance should produce the optimum result.

In all balancing methods discussed, the unbalance influence coefficient must be known prior to balancing. Sometimes it may be undesirable to add a trial weight since its addition may cause larger amplitudes at ω_b. In these cases, the direct method should be used.

References

1 Bishop, R. E. D., "Unbalanced and Initially Bent Shafts," *Engineering*, Nov. 25, 1960, pp. 735–736.

2 Bishop, R. E. D., and Gladwell, G. M. L., "The Vibration and Balancing of an Unbalanced Flexible Rotor," *Journal of Mech. Engineering Science*, Vol. 1, No. 1, 1959, pp. 66–77.

3 Parkinson, A. G., Jackson, K. L., and Bishop, R. E. D., "Some Experiments on the Balancing of Small Flexible Rotors: Part I—Theory," *Journal of Mechanical Engineering Science*, Vol. 5, No. 1, 1963, pp. 114–128.

4 Parkinson, A. G., Jackson, K. L., and Bishop, R. E. D., "Some Experiments on the Balancing of Small Flexible Rotors: Part II—Experiments," *Journal of Mechanical Engineering Science*, Vol. 5, No. 2, 1963, pp. 133–145.

5 Thearle, E. L., "Dynamic Balancing of Rotating Machinery in the Field," TRANS. ASME, Vol. 56, 1934, pp. 745–753.

6 Goodman, T. P., "A Least-Squares Method for Computing Balance Corrections," *Journal of Engineering for Industry*, TRANS. ASME, Series B, Vol. 86, 1964, pp. 273–279.

7 Kellenberger, W., "Balancing Flexible Rotors on Two Generally Flexible Bearings," *Brown Boveri Review*, Sept., 1967.

8 Tessarzik, J. M., Badgley, R. H., and Anderson, W. J., "Flexible Rotor Balancing by the Exact Point-Speed Influence Coefficient Method," ASME Paper No. 71-Vibr.-91.

9 Le Grow, J. W., "Multiplane Balancing of Flexible Rotors—A Method of Calculating Correction Weights," ASME Paper No. 71-Vibr.-52.

10 Lund, J. W., and Jonnesen, J., "Analysis and Experiments on Multi-Plane Balancing of a Flexible Rotor," ASME Paper No. 71-Vibr.-74.

11 Bishop, R. E. D., and Parkinson, A. G., "On the Use of Balancing Machines for Flexible Rotors," *Journal of Engineering for Industry*, TRANS. ASME, Series B, Vol. 94, 1972, pp. 561–576.

12 Kellenberger, W., "Should a Flexible Rotor Be Balanced in N or (N + 2) Planes?" *Journal of Engineering for Industry*, TRANS. ASME, Series B, Vol. 94, 1972, pp. 548–560.

13 Wilcox, J. B., *Dynamic Balancing of Rotating Machinery*, Pitman, London, 1967.

14 Jackson, C., "Using the Orbit to Balance," Mechanical Engineering, Feb., 1971, pp. 28–32.

DISCUSSION[2]

S. Mohan[3]

The authors are to be commended for presenting this excellent paper explaining the effects of residual bow parameters ($\bar{\delta}_y$ and ϕ_y) for a single mass flexible rotor in rigid supports. The applicability of these results to the industrial rotating equipment is somewhat limited because of: *(a)* the inherent assumptions made to simplify the analysis, especially the assumption of rigid bearings and treatment of damping; *(b)* the impracticality of instrumenting the machines at the middle of the shaft for vibration measurement. Authors' comments in this regard would be appreciated.

It is felt that a careful analysis of vibration and phase data is of utmost importance in using the results of this paper. At speeds where the vibration is low (for example $f \approx 0.707$ (Fig. 6) and $f \approx 1.414$ (Fig. 11) it is important to monitor the phase changes carefully. The presence of nonsynchronous vibration components due to gears or misalignment complicates the data analysis further. The movement of the timing mark on the shaft orbit (filtered at running speed) is very useful in such instances. The discusser has come across a number of turbomachines exhibiting response characteristics similar to Fig. 6 as well as Fig. 11. At one particular instance, a response similar to Fig. 6 was recorded at an outboard probe. This response was solely due to an electrical run-out indication at that location and not due to a bowed shaft.

Overall, the paper does give a good feel for explaining the usual phase and response characteristics of industrial turbomachines and thus helps in predicting their reliability with confidence.

[2] Discussion on Paper Nos. 75-GT-48 and 75-GT-49.

[3] Analysis Engineer, Dresser Clark Turbo Products, Dresser Industries, Inc., Olean, New York.

C. Jackson[4]

I will presume this paper(s) is to be selected for the Transactions as it offers both theory and results in the two parts of a common and misunderstood phenomenon noted by many engineers recording rotor response data, or involved in balancing. The typical response would be for the phase mark or angle to shift against the direction of rotation as speed increases, and for the peak amplitude of any critical to occur at the 90 deg shift, and the shift to complete with an 180 deg total shift as the mass center moves forward and the rotor commences to rotate about mass centers rather than geometric centers. Further, one expects to see the displacement of the rotor increase due to the accelerating forces, $Me\ W^2$.

The authors have shown that an existing bow in the rotor causes strange things to happen as outlined in this paper. I would also preclude that multidisk rotors with a determined modal mass should respond in a similar manner, though complicated by other nonlinear reactions such as working friction.

The characteristics of phase shift and reduction with speed of the vibration level, have been noted by me on several occasions. I would like to ask several questions of the authors based on these two papers.

Presuming that a residual bow exists on a rotor, please comment on the effects from a low speed, i.e., 300–500 rpm balance in a balance-machine on a rotor to operate at 8000–10000 rpm. One would expect that correction to apply primarily to the residual bow eccentricity.

In Method II, 75-GT-49, page 4, Fig. 18, please explain the increase in amplitude at the critical, frequency ratio = 1.

Since proximity probes can give an electrical runout of a shaft's surface at low speeds (or high) due to the anomalies in the shaft's surface through one rotation, might not this lead one to a calculated correction that is in error? Take the case where the surface mechanical runout is 0.2 mils by dial indicator yet the eddy current probe indicates 01.0 mils at even a different phase than the mechanical runout.

Another peculiarity could be expected to happen. Should the rotor be honed in the area seen by the probes but after the impellers are shrunk causing some residual bow? The machined area could not only be free of mechanical runout but also electrical runout yet an actual mechanical bow of the rotor exists. I would not expect an answer on this quirk of events; yet, such a thing is possible especially on a repair.

It might be interesting to discuss the Method II advantages, if any, over Method III.

Under Nomenclature of Part I, 75-GT-48, page 2, it was noted that the vector bar was left off the unbalance eccentricity vector, and a vector bar rather than absolute value bar was shown on the nondimensional residual bow ratio.

In equation (43), I found it quite easy to make a mistake by not converting the first term into eccentricity, inches, from the 1/g or 1/oz units generally determined from trial weights. Is the complex residual bow, second term of equation (43) an eccentricity or a peak-to-peak term?

In conclusion, I wish to express my appreciation to Gunter and his staff, Paul Allaire and John Nicholas, for two interesting papers which may well entice our group into a test on a flexible multidisk rotor. I might add that we have only experimented with this solution but it has required that the bow correction weight be necessary to go through the critical on a six mass rotor.

[4] Engineering Fellow, Mechanical Technology Department, Monsanto Polymers & Petrochemicals Co., Texas City, Texas. Mem. ASME.

Author's Closure

The authors wish to express their appreciation of Jackson and Mohan for their interest and comments on this paper.

In response to Jackson's inquiries, a low speed balance to zero amplitude at the center of a rotor with a residual bow could be catastrophic. At low speeds, the rotor amplitude is due almost entirely to the residual bow amplitude (see Fig. 4). In order to balance the rotor amplitude to zero, a very large balance weight would have to be added at the rotor center to counteract the effect of the residual bow (i.e., to unbend the shaft). Using the example suggested by Jackson, consider balancing a bowed rotor at 500 rpm whose operating speed is 10,000 rpm. Assume the rotor critical speed on rigid supports is ω_{cr} = 523.6 rad/s (5000 rpm) and that the rotor has a 5.08×10^{-3} cm (2 mil) bow. For a balance to zero amplitude at ω_b (500 rpm), equation (26) requires that there must be an effective unbalance $\hat{e}_u$ such that

$$\hat{e}_u = -\frac{\alpha_r}{\alpha_u}\hat{\delta}_r$$

Using equations (27) and (28)

$$\hat{e}_u = -\left(\frac{\omega_{cr}}{\omega_b}\right)^2\hat{\delta}_r$$

Using the speed valves suggested here, the magnitude of the unbalance needed to correct the residual bow at 500 rpm is 0.508 cm (200 mils) which is extraordinarily large. Trying to run the rotor up in speed after adding a balance weight to correct for the residual bow would cause tremendously large amplitudes at the critical.

This analysis should not be confused with a rigid body balancing in two planes for multimass rotors. The balancing planes are usually taken at or near the bearings, which in turn are located near the ends of the machine. At the low speeds used for rigid body bal-

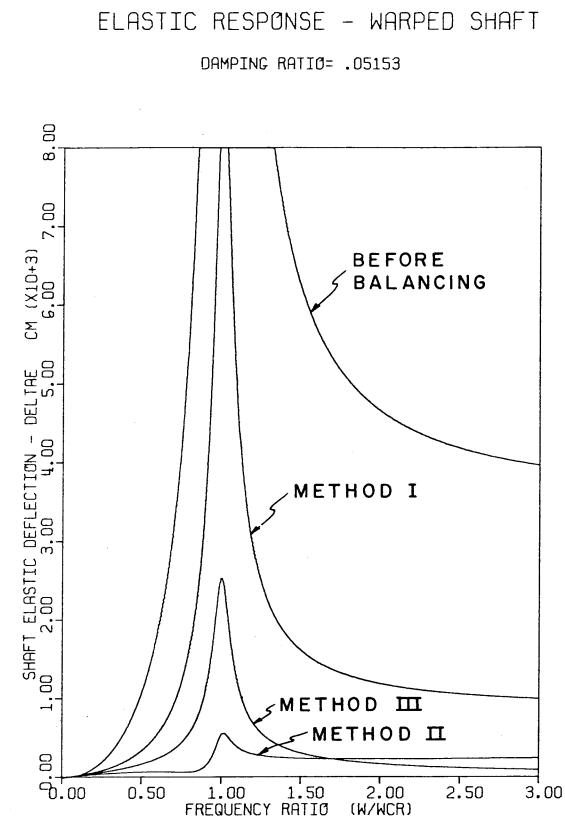

Fig. 22 Elastic response curves before and after balancing a bowed shaft by balancing Methods I, II, and III

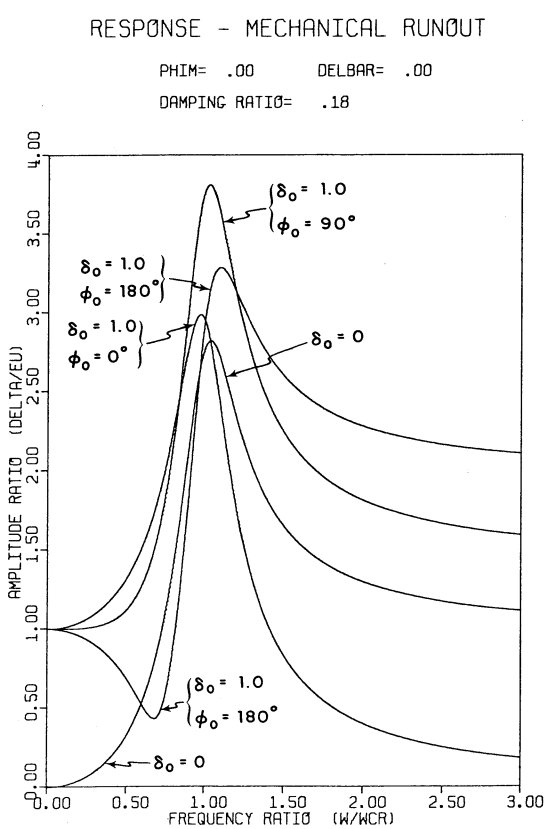

Fig. 23 Response curves with zero residual bow and various values of mechanical runout

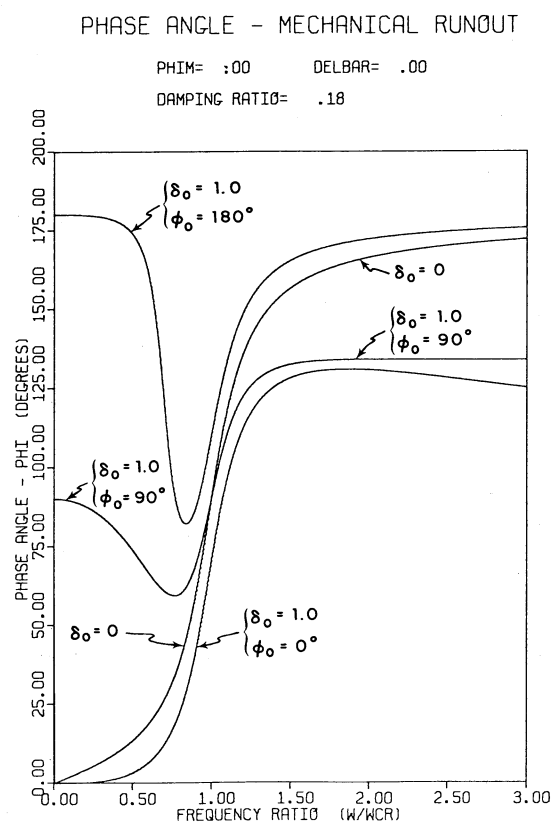

Fig. 24 Phase angle curves with zero residual bow and various values of mechanical runout

ancing, the residual bow looks like an unbalance eccentricity. If the balance weights are placed opposite the residual bow but out near the bearings, the amplitude of vibration and the force will both be greatly reduced at the balance speed. However, since the weights are located near the bearings, they will not excite the first bending mode, as will a single weight at the rotor center.

The approximation used in balancing Method II was that the residual bow influence coefficient, α_r equals 1.0. This, of course is not true as α_r is given by equation (28). This approximation causes the slight rise in amplitude at the critical speed for Method II in Fig. 18.

Fig. 22 shows the elastic response of the shaft before balancing and after balancing by Methods I, II, and III. These are the same curves as shown in Fig. 18 except the residual bow vector was subtracted from the total shaft amplitude leaving only the elastic deflection. If bearing forces and shaft stresses (both proportional to elastic shaft deflection) are considered more critical than total shaft amplitude, Method II is superior to Method III for speeds below, at and slightly above the critical speed.

Figs. 23 and 24 show response and phase angle curves for a rotor with zero residual bow and various values of mechanical runout (amplitude δ_0 and phase ϕ_0). Mechanical runout is a constant runout vector that may be picked up by noncontracting probes due to out-of-roundness of the surface monitored by the probes. Examination of Figs. 23 and 24 reveal that mechanical runout looks very similar to residual bow runout. Frequently, mechanical runout and residual bow runout are both present in a rotor. Furthermore, it may be difficult if not impossible to separate the two effects. In such cases, balancing down to the runout, whether mechanical, residual bow or both, would be recommended. Thus, balancing Method II should be employed. Mechanical runout should be fairly easy to detect by using a dial indicator to measure the surface the noncontacting probe is monitoring. If the surface is perfectly cylindrical, then the mechanical runout is zero.

Electrical runout may also be encountered due to magnetic effects in the shaft or other causes. This usually results in a constant amplitude added to the total shaft amplitude at all phase angles. When no means of determining the exact nature of the low speed probe readings is available, Method II appears to offer the best balancing procedure.

The authors suggest that amplitudes may be measured in peak-to-peak values *or* peak values as long as consistency is maintained throughout all measurements.

The assumptions of a single mass rotor on rigid supports may easily be extended to symmetric, inboard, multimass systems on flexible supports by using a modal mass and effective stiffness and damping coefficients that act at the rotor center. These balancing procedures may be used for balancing out the first bending mode which cannot be accomplished by low speed rigid body balancing.

It is true that it is often impractical to measure the vibration levels at the machine center. Every attempt should be made, however, to monitor the amplitudes at the shaft center since many times this is where the maximum amplitude occurs. In many cases, a critical speed computer program has already been run on a machine. This may be used to infer the amplitude at the rotor center from data taken in other areas if the machine operates near the first bending mode.